

**Reformulation of Coal-Derived Transportation Fuels:
Selective Oxidation of Carbon Monoxide on Metal Foam Catalysts**

Annual Report

Reporting Period Start Date: December 31, 2002

Reporting Period End Date: December 31, 2003

Principal Authors: NC State: Mr. Paul Chin
Dr. George W. Roberts
Dr. James J. Spivey

Clemson: Ms. Amornmart Sirijaruphan
Dr. James G. Goodwin, Jr.
Dr. Richard W. Rice

Date Report Issued: December 31, 2003

DOE Award Number: DE-FG26-O1NT41277

North Carolina State University
Department of Chemical Engineering
Raleigh, NC 27695-7905

Clemson University
Department of Chemical Engineering
Clemson, SC 29634-0909

Porvair Advanced Materials
700 Shepherd Street
Hendersonville, NC 28792

Disclaimer:

This report was prepared as an account of work sponsored by an agency of the United States Government. Neither the United States Government nor any agency thereof, nor any of their employees, makes any warranty, express or implied, or assumes any legal liability or responsibility for the accuracy, completeness, or usefulness of any information, apparatus, product, or process disclosed, or represents that its use would not infringe privately owned rights. Reference herein to any specific commercial product, process, or service by trade name, trademark, manufacturer, or otherwise does not necessarily constitute or imply its endorsement, recommendation, or favoring by the United States Government or any agency thereof. The views and opinions of authors expressed herein do not necessarily state or reflect those of the United States Government or any agency thereof.

NCSU Abstract

Uses for structured catalytic supports, such as ceramic straight-channel monoliths and ceramic foams, have been established for a long time. One of the most prominent examples is the washcoated ceramic monolith as a three-way catalytic converter for gasoline-powered automobiles. A distinct alternative to the ceramic monolith is the metal foam, with potential use in fuel cell-powered automobiles. The metal foams are characterized by their pores per inch (ppi) and density (ρ).

In previous research, using 5 wt% platinum (Pt) and 0.5 wt% iron (Fe) catalysts, washcoated metal foams, 5.08 cm in length and 2.54 cm in diameter, of both varying and similar ppi and ρ were tested for their activity (X_{CO}) and selectivity (S_{CO}) on a CO preferential oxidation (PROX) reaction in the presence of a H₂-rich gas stream. The variances in these metal foams' activity and selectivity were much larger than expected. Other structured supports with 5 wt% Pt, 0-1 wt% Fe weight loading were also examined.

A theory for this phenomenon states that even though these structured supports have a similar nominal catalyst weight loading, only a certain percentage of the Pt/Fe catalyst is exposed on the surface as an active site for CO adsorption. We will use two techniques, pulse chemisorption and temperature programmed desorption (TPD), to characterize our structured supports. Active metal count, metal dispersion, and other calculations will help clarify the causes for the activity and selectivity variations between the supports.

Results on ceramic monoliths show that a higher Fe loading yields a lower dispersion, potentially because of Fe inhibition of the Pt surface for CO adsorption. This theory is used to explain the reason for activity and selectivity differences for varying ppi and ρ metal foams; less active and selective metal foams have a lower Fe loading, which justifies their higher metal dispersion. Data on the CO desorption temperature and average metal crystallite size for TPD are also collected.

Clemson Abstract

Selective oxidation of CO in hydrogen is an important reaction for producing hydrogen from hydrocarbons suitable for use in fuel cells. Pt has been shown to be very active for this reaction. This paper reports on the results of an investigation into the impact of Fe promotion on Pt/ γ -Al₂O₃ using heavily isotopic transient kinetic analysis (ITKA).

In this study, Fe promotion was found to have an impact on activity, selectivity and also time-on-stream behavior of surface reaction parameters. It increased activity and selectivity, as has been also noted by others. ITKA revealed that the higher activity of PtFe is mainly due to an increase in intrinsic site activity when compared to non-promoted Pt. Fe promotion did not affect significantly the total concentration of active intermediates.

In a previous study, Pt/ γ -Al₂O₃ was found to exhibit steady activity for selective CO oxidation after an initial rapid partial deactivation. The PtFe catalyst also showed rapid initial partial deactivation similar to Pt. The activities of both catalysts decreased with time-on-stream about the same degree in reaching a pseudo-steady-state. Unlike for Pt where initial partial deactivation was due primarily to a decrease in active intermediates, the initial rapid partial deactivation for PtFe was the result of both a decrease in the concentration of surface intermediates and a decrease in the average intrinsic site activity, but mainly due to a decrease in the intrinsic site activity. The intrinsic site activity of PtFe approached that of Pt with TOS. It would appear that carbon deposition causes the initial partial deactivation on Pt and may partially do so on PtFe. However, evidence suggests that reoxidation of Fe may also be a significant cause of the loss of activity of PtFe. As partial deactivation proceeds, the effect of Fe promotion of the Pt sites decreases.

Table of Contents

	<u>Page</u>
Disclaimer	ii
NCSU Abstract	iii
Clemson Abstract	iv
Table of Contents	v
List of Graphical Materials	vii
List of Equations and Reactions	ix
1. Introduction	1
1.1 Preferential Oxidation (NCSU)	1
1.2 Motivation (NCSU)	2
1.3 Introduction (Clemson)	4
2. Executive Summary	5
2.1 NCSU Executive Summary	5
2.2 Clemson Executive Summary	5
3. Experimental	7
<i>NCSU</i>	
3.1 Catalyst Support (NCSU)	7
3.2 Experimental Design (NCSU)	7
3.2.1 Equipment and Measurement (NCSU)	7
3.2.2 Reactor Design (NCSU)	9
3.2.3 Process Design (NCSU)	10
3.3 Pulse Chemisorption Run Procedure (NCSU)	11
3.4 Temperature Programmed Desorption Run Procedure (NCSU)	11
<i>Clemson</i>	
3.5 Catalyst Preparation (Clemson)	12
3.6 Catalyst Characterization (Clemson)	13
3.7 Temperature Programmed Reduction (Clemson)	13
3.8 Temperature Programmed Desorption (Clemson)	13
3.9 Reaction System (Clemson)	13
3.10 Reaction Measurements (Clemson)	13
3.11 Isotopic Transient Kinetic Analysis (Clemson)	14
4. NCSU Results and Discussion	15
4.1 CO Pulse Chemisorption	15
4.1.1 Theory	15
4.1.2 Data Analysis	17
4.1.2.1 Standards	17
4.1.2.2 'Identical' Supports	19

4.1.2.3 Varying ppi and ρ Metal Foams	20
4.1.2.4 Varying Fe Ceramic Monoliths	21
4.2 CO Temperature Programmed Desorption	22
4.2.1 Theory	22
4.2.2 Data Analysis	23
4.1.2.1 Standards	23
4.2.2.2 'Identical' Supports	23
4.1.2.3 Varying ppi and ρ Metal Foams	23
4.1.2.4 Varying Fe Ceramic Monoliths	25
5. Clemson Results and Discussion	26
<i>Results</i>	
5.1 Catalyst Characterization	26
5.2 Temperature Programmed Reduction	26
5.3 Temperature Programmed Desorption	26
5.4 Activity Measurement	27
5.5 Isotopic Transient Kinetic Analysis	28
5.6 Characteristics of the Catalyst Surface at Steady State	28
<i>Discussion</i>	
5.7 Chemisorption and TPD Results	29
5.8 Effect on Fe Promotion on Overall Activity	29
5.9 Selectivity	31
5.10 Deactivation Behavior	31
6. Conclusions	33
6.1 NCSU Conclusion	33
6.2 Clemson Conclusion	33
7. Recommendations	35
7.1 NCSU Recommendations	35
7.2 Clemson Recommendations	35
8. References	36
9. Bibliography	39
10. List of Acronyms and Abbreviations	40
Appendices	42
Appendix A: Metal Foam Pictures	43
Appendix B: NCSU Reactor and Process Diagrams	44
Appendix C: Clemson Figures	51
Appendix D: NCSU Pulse Chemisorption Figures	62
Appendix E: NCSU TPD Figures	68

List of Graphical Materials

<u>List of Tables:</u>	<u>Page</u>
Table 3.1: NDIR Components and Ranges	9
Table 4.1: Obtainable results from pulse chemisorption and TPD	15
Table 4.2: Blank reactor data at various N ₂ flow rates	18
Table 4.3: Uncatalysed, unwashcoated blank foam data at various N ₂ flow rates and NDIR span gas cylinders	18
Table 4.4: Chemisorption 'identical' pieces of metal foam intracomparison	19
Table 4.5: Chemisorption comparison of 5 wt% Pt / 0.5 wt% Fe, varying ppi and ρ metal foams	21
Table 4.6: Chemisorption comparison of 400 cpsi, 5 wt% Pt, varying Fe ceramic monoliths	22
Table 4.7: TPD comparison of 5 wt% Pt / 0.5 wt% Fe, varying ppi and ρ metal foams	24
Table 4.8: TPD bimodal peak results for the 20 ppi, 12% ρ metal foam, trial one	25
Table C.1: Characterization results for the Pt and PtFe catalysts.	51
Table C.2: Activity and selectivity of Pt and PtFe at different feed compositions.	51
Table D.1: Uncatalysed, unwashcoated blank foam and blank reactor data	64
Table D.2: 'Identical' pieces of metal foam intracomparison	65
Table D.3: Comparison of 5 wt% Pt / 0.5 wt% Fe, varying ppi and ρ metal foams	66
Table D.4: Comparison of 5 wt% Pt, varying Fe loading ceramic monoliths	67
Table E.1: 'Identical' pieces of metal foam intracomparison	70
Table E.2: Comparison of 5 wt% Pt, varying Fe loading ceramic monoliths	70
Table E.3: Comparison of 5 wt% Pt / 0.5 wt% Fe, varying ppi and ρ metal foams	71
 <u>List of Figures:</u>	
Figure 1.1: CO (a) conversion and (b) selectivity for various ppi and ρ metal foams.	2
Figure 1.2: 5 wt% Pt / 0.5 wt% Fe, 40 ppi 4% ρ 'identical' metal foams intracomparison of (a) CO conversion and (b) CO selectivity	3
Figure 1.3: 5 wt% Pt, varying Fe loading, 400 cpsi ceramic-straight channel monoliths activity & selectivity comparison at (a) $T_{in} = 100^{\circ}\text{C}$ and (b) $T_{in} = 170^{\circ}\text{C}$	3
Figure 3.1: Catalyst support length	7
Figure 3.2: Sample pictures of a (a) 40 ppi, 4% ρ metal foam, (b) 400 cpsi ceramic straight-channel monolith, and (c) 400 cpsi metal monolith	8

	<u>Page</u>
Figure A.1: Different shapes of metal foams.	43
Figure A.2: Metal foams inserted with metal tubes.	43
Figure B.1: Reaction reactor design schematic.	44
Figure B.2: Reaction reactor design dimensions.	45
Figure B.3: Characterization reactor design schematic.	46
Figure B.4: Characterization reactor design dimensions.	47
Figure B.5: Characterization reactor flange and gasket dimensions	48
Figure B.6: Process Flow Diagram	49
Figure C.1: Temperature programmed reduction profiles of Pt and PtFe compared to an Fe catalyst.	53
Figure C.2: Temperature programmed desorption of gas mixture (1%CO, 45% H ₂ in He) on Pt, PtFe and Fe catalyst.	54
Figure C.3: a) CO oxidation rate b) H ₂ oxidation rate and c) CO ₂ selectivity of the Pt and PtFe catalysts.	55
Figure C.4: Effect of pre-exposing to a stream of O ₂ /He or CO/He on a) Pt and b) PtFe catalysts.	56
Figure C.5: Typical normalized transient response.	57
Figure C.6: Time-on-stream behavior of a) the pseudo-first-order intrinsic rate constant and b) concentration of surface CO ₂ intermediates of Pt and PtFe for P _{O₂} =1.8 kPa.	58
Figure C.7: Amount of carbon deposited on PtFe with time-on-stream.	59
Figure C.8: a) Rate constant distribution b) shift of total CO ₂ intermediates of the PtFe catalyst at different time-on-streams.	60
Figure C.9: Rate constant distribution of the Pt and PtFe catalysts at a) 5 min TOS and b) steady state.	61
Figure D.1: Graphical representation of a theoretical pulse chemisorption test	62
Figure D.2: Graphical representation of a typical theoretical pulse chemisorption data.	62
Figure D.3: Graphical representation of a pulse chemisorption test with elongated tails	63
Figure D.4: Graphical representation of an elongated pulse chemisorption data.	63
Figure E.1: Typical graphical representation of TPD data.	68
Figure E.2: Bimodal peak TPD graph for the 20 ppi, 12% ρ metal foam, trial one	69

List of Equations and Reactions

List of Equations:

	<u>Section</u>	<u>Page</u>
E1: Moles of CO in sample loop	4.1.1	16
E2: Total moles of CO adsorbed by the active metal	4.1.1	16
E3: Moles of active metal adsorbing CO	4.1.1	16
E4: Metal dispersion calculation	4.1.1	17
E5: Average metal crystallite size	4.1.1	17
E6: Error associated with the number of moles of CO in the pulse and the integrated NDIR reading	4.1.2.1	18

List of Reactions:

(R1): Carbon monoxide oxidation reaction	1.1	1
(R2): Hydrogen oxidation reaction	1.1	1
(R3): Water-gas-shift reaction	1.1	1

1. Introduction

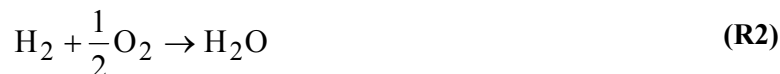
1.1 Preferential Oxidation (NCSU)

The development of practical fuel cell power for both automotive transportation and stationary applications will require the development of fuel processors that convert liquid fuels into hydrogen and carbon dioxide. Fuel processors must be compact, mechanically durable, quick-starting, responsive to transient demands, and inexpensive.

The inlet gas stream fed to the fuel cell must have a very low concentration of CO to avoid poisoning the fuel cell electrode^{1,2}. The final selective oxidation step requires a catalyst that is active for the oxidation of CO (reaction R1) in order to reduce the concentration of CO from ~1% to less than 10 ppm in the presence of high concentrations of H₂, CO₂, and steam, using a minimum volume of catalyst.



However, the catalyst must not oxidize a significant quantity of hydrogen (reaction R2)



since H₂ is the fuel used at the anode of the fuel cell, nor should it have a strong preference to the water-gas-shift reaction (reaction R3). Hydrogen consumed by reaction R2 during the selective oxidation step must be replaced by increasing the size of the fuel processor, and increasing the rate of feed to the fuel processor. Therefore, the catalyst must be highly active for the oxidation of CO and highly selective for reaction R1 over reaction R2. The process described above is known as “preferential oxidation” in the fuel cell community, and is often referred to using the acronym “PROX”.

Previous CO PROX research accomplished under this grant used metal foams and ceramic monoliths washcoated with γ -Al₂O₃ containing 5 wt% Pt and 0-1 wt% Fe nominal loadings. A 400 cpsi ceramic straight-channel monolith support with a 5 wt% Pt / 0.5 wt% Fe loading proved to have a high activity for CO conversion, along with a moderate selectivity for CO over H₂. With an inlet temperature of 100°C, 1.0% CO, and an O₂/CO ratio = 1.0 in the feed gas, this catalyst was able to achieve ~80% conversion and ~40% selectivity. The CO selectivity could only reach a maximum of 50% for complete oxidation because the test was carried out at double the stoichiometric concentrations of O₂.

Tests were conducted on metal foams with a 5 wt% Pt / 0.5% Fe / γ -Al₂O₃. The best metal foam structure was the 40 ppi, 4% ρ . Catalysts prepared on this metal foam had comparable activity and selectivity to the 400 cpsi ceramic monolith. The activity and

selectivity of the metal foams with 5 wt% Pt / 0.5 wt% Fe ranked from highest to lowest are as follows:

$$40 \text{ ppi, } 4\% \rho > 20 \text{ ppi, } 4\% \rho > 20 \text{ ppi, } 12\% \rho > 40 \text{ ppi, } 12\% \rho$$

Studies on catalyst prepared with the 5 wt% Pt / 0.5 wt% Fe washcoat showed that the reverse water-gas-shift (r-WGS) reaction played an important role in determining CO conversion and selectivity, especially at higher inlet temperatures. This reaction needs to be suppressed to reach feasible CO concentrations.

1.2 Motivation (NCSU)

As mentioned in section 1.1, CO PROX reactions were conducted for metal foams and ceramic monoliths for their activity and selectivity. For varying ppi and ρ metal foams washcoated with 5 wt% Pt and 0.5 wt% Fe, the activity and selectivity varied greatly between the catalysts, as shown in Figure 1.1.

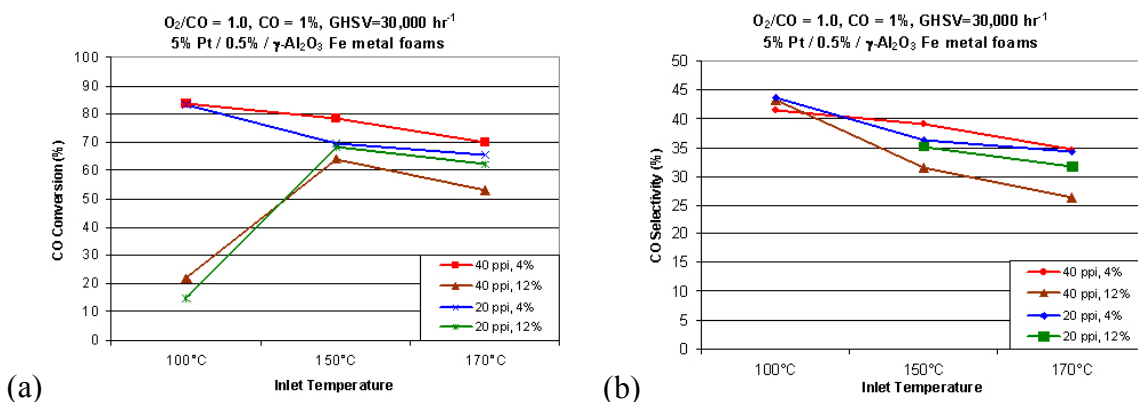


Figure 1.1: CO (a) conversion and (b) selectivity for various ppi and ρ metal foams.

Even with different ppi and ρ , the activity and selectivity of these catalyst should not vary so greatly, especially the CO conversion of the 12% ρ metal foams at $T=100^\circ\text{C}$. One explanation for this variable behavior is that even though the nominal metal weight loadings on the metal foams are the same, each metal foam has a different number of active metal sites for CO to adsorb on to its surface.

Multiple operating conditions were examined in the PROX reaction, such as gas hourly space velocity and linear velocity. Studies done on three ‘identical’ pieces of support showed that the performance of the supports prepared on either the ceramic monolith or metal foam was influenced by mass and heat transport. The identical pieces all had 5 wt% Pt, 0.5 wt% Fe, 1.6 g/in^3 gross catalyst volume washcoat loading, 5.08 cm in length and 2.54 cm in diameter, and either 40 ppi 4% ρ , or 400 cpsi.

When each of the individual ‘identical’ pieces of support was tested, their activity and selectivity differed. Again, the explanation of varying number of active metal sites for

CO adsorption on each ‘identical’ support can account for the difference in activity and selectivity of the ‘identical’ pieces of metal foams and ceramic monoliths. The metal foam intracomparison is shown in Figure 1.2.

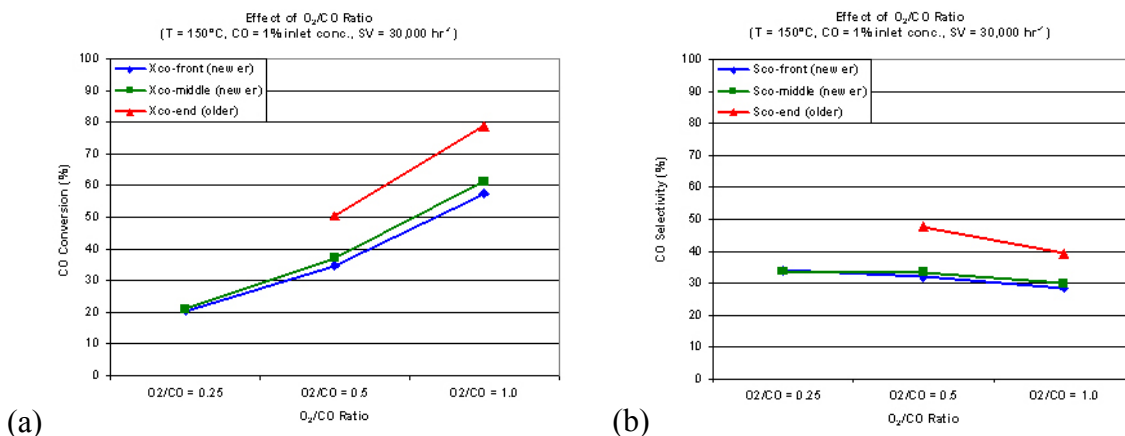


Figure 1.2: 5 wt% Pt / 0.5 wt% Fe, 40 ppi 4% ρ ‘identical’ metal foams intracomparison of (a) CO conversion and (b) CO selectivity

The CO PROX reaction conducted on 5 wt% ceramic monoliths contained four different Fe loadings: 0 wt%, 0.05 wt%, 0.5 wt%, and 1.0 wt%. At T_{in}=170°C, the activity and selectivity were independent of Fe loading, illustrated on Figure 1.3b. At T_{in}=100°C, the differences were more distinct because of incomplete oxidation. The use of catalyst characterization on the various Fe ceramic monoliths will help distinguish the role of Fe promotion on Pt as it influences their activity and selectivity.

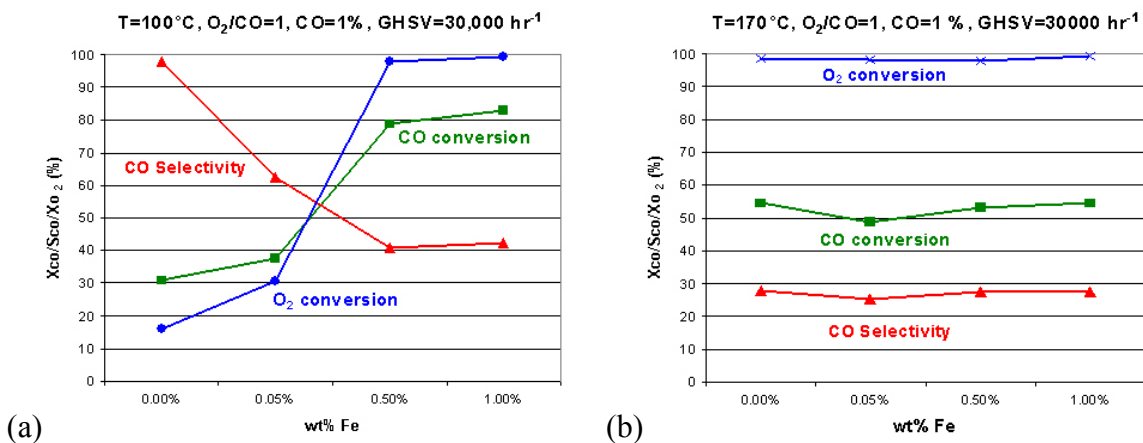


Figure 1.3: 5 wt% Pt, varying Fe loading, 400 cpsi ceramic-straight channel monoliths activity & selectivity comparison at (a) T_{in} = 100°C and (b) T_{in} = 170°C

To determine the number of active metal sites for CO adsorption on our supports, amongst other characteristics, catalyst characterization must be employed. The characterization of the catalytic supports should elucidate the cause for the variance seen in the varying ppi and ρ metal foams, the ‘identical’ pieces of support, and the varying Fe

loading on ceramic monoliths. Our research utilizes two techniques to accomplish this task: pulse chemisorption and temperature programmed desorption (TPD).

1.3 Introduction (Clemson)

Poisoning by CO impurities of the electrode in a proton exchange membrane fuel cell is a potential problem in using hydrogen derived from hydrocarbons by reforming or partial oxidation. In order to reduce the amount of CO in the hydrogen stream to a tolerable level (<10 ppm) without sacrificing too much hydrogen, a suitable catalyst must be used downstream of hydrogen generation to convert the CO to CO₂. Pt/alumina has been found to be suitable for this purpose^{3,4}. Unfortunately, rapid partial deactivation during the initial reaction period at desired low reaction temperatures makes the catalyst much less active and selective than it could be. Our previous work⁵ showed that the adsorption of CO is more favorable on the Pt surface than either oxygen or hydrogen. We suggested that the imbalance between the amounts of CO and O₂ adsorbed on the catalyst surface at typical reaction conditions might be the main reason for coke formation, the apparent cause of the initial deactivation to steady-state reaction. Carbon removal by reaction with either oxygen or hydrogen in the reactant stream is not sufficient to prevent carbon build up on the initial catalyst surface.

There have been several investigations reported of the effects of promoters (Fe oxide, ceria) on the activity and selectivity of Pt/alumina⁶⁻⁸. Korotkikh and Farrauto⁶ studied the effect of Fe oxide promotion on Pt/alumina powdered catalysts and monolith catalysts. They found that with Fe oxide promotion, CO conversion increased significantly but the selectivities remained relatively constant. In a following paper, Fe promoted Pt/alumina catalyst was studied in detail⁷. A non-competitive dual site mechanism for the selective oxidation of CO was proposed. The promoted Pt catalyst was suggested to be more active due to Fe oxide providing adsorption sites for oxygen with Pt providing adsorption sites for carbon monoxide. The effect of ceria on a Pt/ γ -Al₂O₃ catalyst was studied by Son and Lane⁸. The ceria-promoted catalyst gave higher conversion and selectivity than Pt alone at low temperature (~100°C). A smaller effect was obtained when the O₂-to-CO ratio was increased.

In this study, the effects of Fe promotion of Pt/alumina on the surface reaction parameters during the selective oxidation of CO were investigated using isotopic transient kinetic analysis (ITKA). From the reaction and ITKA results, the effect of Fe promotion on the apparent activity, the intrinsic "site" activity, and the concentration of active intermediates was able to be determined. The evolution of the site activity distribution with time-on-stream was also determined.

2. Executive Summary

2.1 NCSU Executive Summary

CO PROX reactions were conducted for metal foams and ceramic straight-channel monoliths for their activity and selectivity. For varying ppi and ρ metal foams washcoated with 5 wt% Pt and 0.5 wt% Fe, the activity and selectivity varied greatly between the catalysts, as shown in Figure 1.1. Similar differences were seen on catalysts with 'identical' ppi and ρ metal foams, and 400 cpsi ceramic straight-channel monoliths with varying Fe loading. Catalyst characterization, mainly pulse chemisorption and TPD, is used to explain the differences seen in their activity and selectivity.

Results on the unwashcoated, uncatalysed blank foam and blank reactor show no uptake of CO. An elongated tail caused by CO bleeding off the support is found on all catalysed, washcoated support pulse chemisorption data. This tail is associated with the Fe, γ -Al₂O₃ washcoat and its surface impurities, or both, weakly chemisorbing or physisorbing CO.

Results on the 5 wt% Pt, 0.5 wt% Fe 'identical' 40 ppi, 4% ρ metal foams show no significant differences in active metal count and metal dispersion, but the dispersions were low, ~5% for both pulse chemisorption and TPD data.

Results on the varying Fe loading on ceramic straight-channel monoliths show that lower Fe correlates to higher dispersion because of a decrease in inhibition of the Pt surface. Therefore, a lower Fe loading on the 12% ρ metal foams is postulated to explain the decrease in dispersion for the more active and selective 4% ρ metal foams in both pulse chemisorption and TPD calculations.

Results on TPD also measure the CO desorption temperature and average Pt crystallite size. The CO desorption temperature data falls into a similar range measured by Manasilp and Gulari. The average Pt crystallite size results for Fe-promoted Pt/ γ -Al₂O₃ are higher than Liu et al and Sakamoto et al, indicating possible sintering of the catalysts by agglomeration. TPD results are lower than the pulse chemisorption results because of CO adsorption on Pt vs. both Pt and Fe, respectively.

Inconsistent results arise for different trials using the same catalyst under identical conditions for both pulse chemisorption and TPD. In TPD, the 20 ppi, 12% ρ metal foam, first trial, produced a bimodal peak that is unexplainable and irreproducible.

2.2 Clemson Executive Summary

Temperature programmed reduction results observed the Pt catalyst to show only one reduction peak at ~218°C. Two reduction peaks were observed for the PtFe catalyst, as expected. The first peak represents platinum oxide reduction and perhaps some catalytic reduction of iron. The second peak at ~290°C is the catalytic reduction of iron oxide. Comparing these results to the results for an Fe/ γ -Al₂O₃ catalyst that exhibited 2

reduction peaks at 377 and 464°C, it is obvious that Pt decreases the reduction temperature required for iron oxide as a result of hydrogen spillover.

Temperature programmed desorption results showed that both Pt and PtFe gave similar desorption behavior except for methane, where the peak was shifted slightly. Surprisingly, no peak for the desorption of CO was observed for any of the catalysts, but there was a peak for CO₂ desorption at ca. 320°C for Pt and PtFe, and at ca. 180°C for Fe, indicating the higher activity of Fe for the Boudourd reaction. There was a broad peak for H₂ desorption starting at 220°C with a peak around 600°C that was essentially identical for Pt, PtFe, and Fe.

The PtFe catalyst was tested for its activity and selectivity and compared to that for the non-promoted Pt catalyst. The space velocity used was four times that used for the non-promoted catalyst in order to have differential conversion at steady state. The CO oxidation rates of both catalysts dropped significantly with TOS. An increase in H₂ oxidation rate was detected for Pt reflecting the decrease in %CO₂ selectivity. Although rate of H₂ oxidation increased with TOS, it was not significant compared to the rapid decrease in rate of CO oxidation resulting in the rapid decrease in total oxidation rate. PtFe showed an opposite change in H₂ oxidation rate. Decrease in H₂ oxidation rate along with CO oxidation rate resulted in a slower decrease in %CO₂ selectivity.

The power law expression for CO oxidation on both catalysts was determined. The approach we used has been described by Kahlich et al.⁹. At $\lambda=2$ and steady state operation, the reaction orders for the power law form of the rate expression for Pt were found to be +1 and 0 for O₂ and CO, respectively. The PtFe catalyst had reaction orders of 0 and 0.2 for O₂ and CO, respectively. This change in reaction order for O₂ indicates the impact of Fe promotion on the mechanism or at least the surface adsorption parameters.

Pt and PtFe showed different deactivation behavior considering the intrinsic site activity, k , and the concentration of active intermediates, N_{I-CO_2} . As deactivation progressed, the intrinsic site activity of Pt remained relatively constant, whereas, for PtFe it decreased significantly. On the other hand, the concentration of active intermediates for Pt decreased more rapidly with TOS compared to that for PtFe. With TOS, the site activity of PtFe appeared to asymptotically approach that of Pt indicating that its surface was becoming more like that of Pt with significantly deactivation.

3. Experimental

3.1 Catalyst Support (NCSU)

Our catalyst supports are cylindrically shaped, with a 2.54 cm inner diameter, and 5.08 cm in length, as shown in Figure 3.1. The supports were supplied by Porvair Fuel Cell Technology (PCFT), in Hendersonville, NC. A series of Fe-promoted Pt catalysts were synthesized and washcoated onto the supports by Environex Inc., in Devon, PA, with a washcoat loading of approximately 1.6 g cat/in³ gross catalyst support volume.

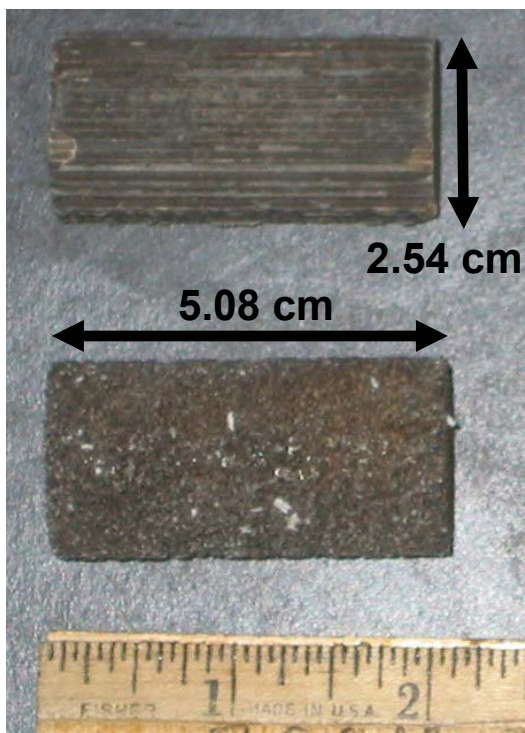


Figure 3.1: Catalyst support length

Four different types of support were tested: metal foams, ceramic straight-channel monoliths, ceramic foams, and corrugated metallic monoliths. Foams have two defining characteristics: pores per inch (ppi) and cell density (ρ). Monoliths are defined by their cells per square inch (cpsi).

Pores per inch is the number of pores in the foam per given inch; a 20 ppi foam has larger channel sizes compared to a 40 ppi foam. Higher ppi foams have greater tortuosity for the fluid flow path. Cell density is the percent value of the actual volume of the foam divided by the total volume of the foam. Cell density is the converse of void volume; a foam with 12% ρ has a void volume of 88%.

Cells per square inch is characterized by the number of cells per given square inch; for a given volume of monolithic support, a 400 cpsi ceramic straight-channel monolith has

smaller channels than a 200 cpsi ceramic straight-channel monolith. Metallic monoliths are fashioned out of spiral-wound corrugated metal supports with a repeating pattern of ~ 3 mm. This results in an open face that is roughly equivalent to a 400 cpsi straight-channel monolith. Examples of different supports are provided in Figure 3.2.

3.2 Experimental Design (NCSU)

3.2.1 Equipment and Measurement (NCSU)

The experimental gases required for the reaction are CO, H₂, O₂, CO₂, H₂O, and N₂. The gas cylinders used for the reaction experiments are: 10% CO in balance N₂, 10% O₂ in balance N₂, 17.6% CO₂ in balance H₂, and pure N₂. The H₂O is supplied via HPLC pump. The gas cylinder compositions were chosen because of safety, compatibility, and lower explosive limit (LEL) levels.

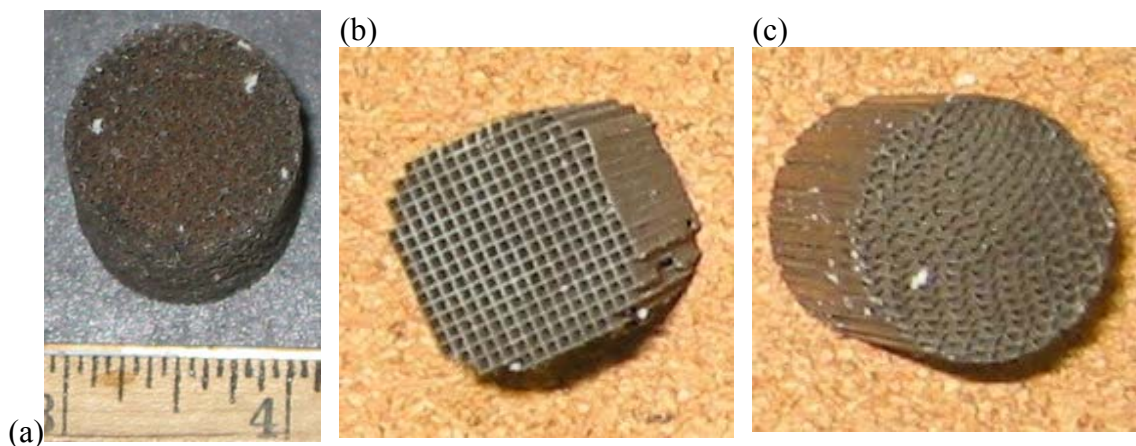


Figure 3.2: Sample pictures of a (a) 40 ppi, 4% ρ metal foam, (b) 400 cps ceramic straight-channel monolith, and (c) 400 cps metal monolith

Gas cylinder flowrates were controlled by Brooks Instrument Model 5850E mass flow controllers. The maximum flow rates for 10% CO in balance N₂, 10% O₂ in balance N₂, 17.6% CO₂ in balance H₂, and pure N₂ are 3500 standard cubic centimeter per minute (scm), 3500 scm, 16000 scm, and 5500 scm, respectively. The mass flow controllers are controlled by a Brooks Instrument Model 5878 control and read out equipment for thermal mass flowmeters. A LabAlliance series 1500 constant flow HPLC pump controlled the flowrate of deionized (DI) water.

The gases are initially heated by an Omega FSB-1 fluidized sand bath, with a maximum heating temperature of 350°C. Additional heating is provided by heating tapes from various companies, such as Omega Engineering, Inc., with a typical maximum heating temperature of 482°C (900°F). The heating tapes are controlled by Variac Voltmeter transformers.

A model 3080SS thermoelectric two channel gas sample chiller, from Universal Analyzers, Inc., is used to cool down the gas stream exiting the reactor to 4°C. This step is required to remove water from the system before entering the gas analyzer.

A Precision Scientific catalog # 63126 wet test meter is used to verify the mass flow controllers' flowrates and as a vent stream. An Omega FL-1345-G variable area rotameter is used to gauge the gas stream flowrate directly prior to the gas analyzer.

A California Analytical Instruments, Inc. (CAI) nondispersive infrared (NDIR) gas analyzer model 300 is used to determine the CO and O₂ concentration. The NDIR has three components, each with four ranges listed on Table 3.1. Each component requires a range of 0.5 – 2.0 L/min of gas to be accurate. There are two inlet gas streams; components 2 and 3 are coupled into the same inlet gas stream, requiring a higher flowrate than component 1. The NDIR is interfaced with a personal computer through a PCI-DAS6025 and CIO-MINI50 boards from Measurement Computing. Data acquisition is done using LabTech Notebook software package.

	Component 1 <i>Carbon Monoxide</i>	Component 2 <i>Carbon Monoxide</i>	Component 3 <i>Oxygen</i>
Range 1	0 – 3000 ppm	0 – 200 ppm	0.000 – 1.000%
Range 2	0.000 – 1.500%	0 – 1000 ppm	0.00 – 15.00%
Range 3	--	--	0.0 – 25.0%
Range 4	--	--	--

Table 3.1: NDIR Components and Ranges

In addition to the NDIR analyzer, there is a Perkins-Elmer Autosystem on-line gas chromatograph: a dual-column, temperature-programmable instrument, equipped with both a thermal conductivity detector (TCD) and a flame ionization detector (FID). The chromatograph is interfaced with a personal computer and the Turbochrom 4 software package is used for data acquisition.

For the pulse chemisorption and TPD, a Valco 6-port manual switching valve, product # 6UWE with 1/8" connections, 400 psi and 225°C maximum pressure and temperature rating, respectively, is used. Three sample loops (1, 2, and 5 mL, product # SL1KUW, SL2KUW, and SL5KUW, respectively) from Valco are used in conjunction with the switching valve.

Thermocouples and pressure indicators are dispersed throughout the process. The thermocouples are monitored by an Omega model CN 101 and 102 high temperature and low temperature alarm monitors, respectively. The reactor inlet and outlet temperatures are controlled and monitored, respectively, by a Yokogawa model UT-14 digital indicating controller. The pressure drop across the support is measured by an Omega model DP41-E 1/8" high performance process indicator.

The process system has 3 gas monitors: two MSA series 5000 CO gas monitor systems, and one MSA series 5000 combustible gas monitor system. The walk-in hood contains one CO and one combustible monitor. The lab contains one CO monitor. All 3 gas monitors are interfaced with a MSA model 5300 monitoring system with warning, caution, and alarm settings.

3.2.2 Reactor Design (NCSU)

The reactor consists of 316/316L stainless steel tubing: 30.48 cm length and 2.8575 cm diameter pipe (3.175 cm tube). An inlet and outlet thermocouple in the reactor measures the inlet and outlet gas stream temperature, respectively, using 18" K-type Omega quick disconnect thermocouples with miniature connectors. Pressure is measured in the reactor, along with the pressure drop across the catalytic support. The pressure in the reactor is controlled by a Tescom back pressure regulator (BPR) downstream of the reactor. Two ceramic foam distributors are placed in the inlet and the outlet of the reactor to help evenly distribute the gas stream.

The reactor is held as close to adiabatic as possible. The 2.54 cm diameter support is wrapped with a low thermal conductivity aluminum oxide ULTRA-TEMP ceramic tape

insulation supplied by McMaster-Carr. The outside reactor tube is first wrapped with insulation foam, and then wrapped with multiple layers of Fisher Scientific fiberglass cloth tape to minimize heat loss from the exothermic heat of reaction. The reactor is then wrapped with heating tape to help maintain the temperature of the reactor, and rewrapped with more fiberglass cloth tape to suppress heat loss from the heating tapes. Finally, aluminum foil is wrapped around the reactor.

The reactor is connected to the rest of the process two different ways. For the reaction system, 2.8575 cm Swagelok male-female threaded connections were used. A schematic of this reactor design can be found in Figures B.1 and B.2 in Appendix B. For the characterization system, when the threaded system could not maintain pressure, the Swagelok threaded connections were replaced with four A-351 MSS 150-lbs A370 SC flanges with 3.175 cm I.D. / 10.795 cm OD, and two McMaster-Carr 1.25" ID / 2.625" OD pure graphite spiral-wound gaskets. A schematic of this reactor design can be found in Figures B.3, B.4, and B.5 in Appendix B.

3.2.3 Process Design (NCSU)

The four gas cylinders containing CO, O₂, H₂, CO₂, and N₂ are piped up using ¼" Swagelok tubing from the gas station located outside on the ground floor. The CO in balance N₂ and O₂ in balance N₂ lines flow through activated carbon (AC) traps before being piped up to the walk-in hood. All lines except for the pure N₂ line are fail closed; the pure N₂ is fail open and interconnected with the other lines in case of failure. The CO₂ in H₂ line has an extra vent to the atmosphere in case of an overpressure. The lines are piped from the gas station to the walk-in hood on the third floor.

From the walk-in hood, the gas flow rates are controlled by mass flow controllers. The pure N₂ and CO₂ in H₂ lines flow through an Alltech Oxytrap to trap oxygen. All four lines have pressure relief valves in case of extreme overpressure. The four gas lines enter Swagelok crosses which act as a mixing bowl for the gas streams. A HPLC pump introduces liquid water into the system downstream of the gas stream mixing. This stream enters the FSB, where it is heated and the water is vaporized. Downstream of the FSB the gas stream maintains its temperature through heating tapes. Fiberglass cloth tape and aluminum foil are used wherever heating tapes are used to decrease the exposure of the heating tapes to the skin in the case of accidental touching, reducing the possibility of severe burning.

For the catalyst characterization techniques, the gas stream flows through a GC sampling valve, where CO can be pulsed into the system before the reactor. For the reaction system, the gas stream is flowed straight into the reactor. The gas stream continues through the reactor and passes through a BPR. Part of the gas stream is removed out to a steam trap before leaving through the first vent. The rest of the gas stream enters a 7 µm particle filter before entering the cooling system. The cooling system cools the remaining gas stream to 4°C.

The remaining gas stream is split into three lines: the first line passes through the wet test meter and acts as a second vent line, the second line operates as the GC inlet gas stream,

and the third line operates as the NDIR inlet gas streams. A rotameter is used to estimate the gas stream flow rate entering the NDIR gas analyzer. This NDIR inlet stream is split into because of the two inlets for the NDIR, as described in section 3.2.2 above. After the GC and NDIR, the outlet streams are vented.

A schematic of the process flow can be found in Figure B.6 in Appendix B.

3.3 Pulse Chemisorption Run Procedure (NCSU)

H₂ reduction / N₂ inert pretreatment

- 1) Turn on pure N₂ line to 90.0% MFC opening (4950 sccm out of 5500 sccm)
- 2) Turn on pure H₂ line to 5.0% MFC opening (800 sccm out of 16000 sccm)
- 3) Set pretreatment temperature to 250°C on reactor inlet (Yokogawa controller)
- 4) Change settings on Variac Voltmeters (VV) and Fluidized Sand Bath (FSB)

FSB =	8.0	VV T3 =	46 V
VV T1 =	48 V	VV T4 =	42 V
VV T2 =	46 V	VV T5 =	46 V

- 5) Run pretreatment for 3 hours (1 hour heating start-up, 2 hours run)
- 6) Shut off pure H₂ line and lower pure N₂ line to 60% MFC opening (3300 sccm)
- 7) Run N₂ pretreatment for 1 hour to purge the surface of the catalytic support

CO Pulse Chemisorption

- 8) Ramp temperature to 40°C on reactor inlet for pulse chemisorption runs
- 9) Turn on chemisorption gas (10% CO in N₂ balance cylinder) and open valve

FSB =	1.5	VV T3 =	13 V
VV T1 =	14 V	VV T4 =	15 V
VV T2 =	14 V	VV T5 =	15 V

- 10) After finished, shut of all VV and FSB and let cool down to ambient temperature
- 11) Shut down all valves and gas in chemisorption and reactor lines

3.4 Temperature Programmed Desorption Run Procedure (NCSU)

H₂ reduction / N₂ inert pretreatment

- 1) Turn on pure N₂ line to 90.0% MFC opening (4950 sccm out of 5500 sccm)
- 2) Turn on pure H₂ line to 5.0% MFC opening (800 sccm out of 16000 sccm)

$$\frac{800 \text{ sccm H}_2}{800 \text{ sccm H}_2 + 4950 \text{ sccm N}_2} = 13.9\% \text{ H}_2 \text{ in N}_2 \text{ balance}$$

- 3) Set pretreatment temperature to 250°C on reactor inlet (Yokogawa controller)
- 4) Change settings on Variac Voltmeters (VV) and Fluidized Sand Bath (FSB)

FSB =	8.0	VV T3 =	46 V
VV T1 =	48 V	VV T4 =	42 V
VV T2 =	46 V	VV T5 =	46 V

- 5) Run H₂ reduction pretreatment for 3 hours (1 hour heating start-up, 2 hours run)
- 6) Shut off pure H₂ line and lower pure N₂ line to 60% MFC opening (3300 sccm)
- 7) Run N₂ pretreatment for 1 hour to purge the surface of the catalyst support

Active Site Saturation

- 8) Ramp temperature to 40°C on reactor inlet for runs

FSB =	1.5	VV T3 =	13 V
VV T1 =	14 V	VV T4 =	15 V
VV T2 =	14 V	VV T5 =	15 V

- 9) Turn on 10% CO in N₂ gas line (from Gas Station) at MFC = 28.6% (1.0 L/min) for 1 hour to saturate all active sites on the catalyst
- 10) Turn off 10% CO in N₂ gas line and run pure N₂ (18.2% MFC, 1.0 L/min)
- 11) Leave pure N₂ gas on *overnight* at reactor temperature of 40°C

TPD

- 12) Make sure temperature is at 40°C on reactor inlet
- 13) Ramp temperature up for experiments running pure N₂ (Gas Station, MFC = 18.2% or 1.0 L/min).

FSB =	9.0	VV T3 =	50 V
VV T1 =	50 V	VV T4 =	42 V
VV T2 =	50 V	VV T5 =	50 V

- 14) After finished, ramp down reactor to ambient temperature
- 15) Shut down all valves and gas and reactor lines

3.5 Catalyst Preparation (Clemson)

A catalyst consisting of 5 wt% Pt on γ -Al₂O₃ powder was prepared according to the procedure described earlier in the previous study⁵. This catalyst is referred to as the “Pt” catalyst through the paper.

To prepare 0.5 wt% Fe + 5 wt% Pt on γ -Al₂O₃ powder, a portion of the 5 wt% Pt on γ -Al₂O₃ powder after calcination was impregnated with an Fe(NO₃)₃•9H₂O solution. The catalyst was then recalcined at 300°C for 2 h. This catalyst is referred to as “PtFe”.

A 0.5 wt% Fe on γ -Al₂O₃ catalyst was also prepared for comparison purposes. Calcined γ -Al₂O₃ was impregnated to incipient wetness with an Fe(NO₃)₃•9H₂O solution dried and then calcined at 300°C for 2 h. This catalyst is referred to as “Fe”.

3.6 Catalyst Characterization (Clemson)

BET surface area measurement, static H₂ and CO chemisorption were performed according to the procedures provided in our previous work⁵. Even though the amount of Fe by weight seems to be small compared to the amount of Pt, it is significant in term of atomic percent. Therefore, we report % dispersion calculated both with and without considering Fe.

3.7 Temperature Programmed Reduction (Clemson)

The reducibilities of the calcined Pt, PtFe and Fe catalysts were measured by temperature programmed reduction using an Altamira AMI-1 system. TPR used a temperature ramp of 5°C /min from 40 to 700°C in a flow of 5% H₂ in Ar. H₂ consumption was measured by analyzing the effluent gas with a thermal conductivity detector. The detector output was calibrated by reduction of Ag₂O powder.

3.8 Temperature Programmed Desorption (Clemson)

For the temperature programmed desorption studies, approximately 50 mg of a calcined catalyst sample was reduced in a stream of hydrogen for 1 h at 550°C. The catalyst was then cooled down to 300°C where it was purged with He and further cooled down to room temperature. In order to measure how CO and H₂ competitively adsorbs in the presence of the other, a gas mixture of 1% CO and 45% H₂ in He was used in this study. The catalyst sample was saturated with this gas mixture at room temperature for 40 min and then purged with He at the same temperature for 30 min before heating up to 700°C at 10°C/min ramp rate. The amounts and species of effluent gases were detected using a Pfeiffer Vacuum Prisma mass spectrometer.

3.9 Reaction System (Clemson)

The design of ITKA reaction systems, such as used in this study, have been shown elsewhere^{10, 11}. Details of the particular system used for this reaction was described in our previous study⁵. The product stream was analyzed using an on-line Varian (CP-3380) with a carbosphere column. Hydrogen, carbon monoxide, and oxygen were first separated at 50°C and then after 5 min the GC was ramped to 150°C at 15°C/min to determine the concentration of CO₂.

3.10 Reaction Measurements (Clemson)

The catalytic activity of the catalyst for the selective oxidation of CO in the presence of hydrogen was determined at 90°C and 1.8 atm. Prior to CO oxidation, approximately 50 mg of Pt or 25 mg of PtFe catalyst was diluted with α -alumina and reduced in-situ in a stream of hydrogen at 550°C for 1 h. After reduction, the temperature was gradually decreased over 4 h to the reaction temperature, at which time the flow was switched to a feed stream containing 45% H₂, 1% O₂, 1% CO and 53% He. Total gas space velocities

of $\sim 190,000 \text{ h}^{-1}$ (100 cc/min) and $760,000 \text{ h}^{-1}$ (200 cc/min) were used for Pt and PtFe catalysts, respectively, to produce differential conversions at steady state. The CO conversion and selectivity were determined periodically until the reaction reached steady state and were calculated using the method described by Manasilp and Gulari⁴. CO₂ selectivity (%CO₂) basically represents the percentage of O₂ reacted with CO rather than with H₂.

3.11 Isotopic Transient Kinetic Analysis (Clemson)

Isotopic transients were measured after switching between isotopically labeled CO (¹²CO vs. ¹³CO). A trace of argon was present in the ¹²CO stream to determine the gas phase holdup in the reaction system. The transient responses of the old isotopically labeled and the new labeled CO₂ and CO exiting the reactor were monitored by a mass spectrometer (Pfeiffer Vacuum Prisma) equipped with a high-speed data acquisition system interfaced to a personal computer using Balzers Quadstar 422 v 6.0 software. The surface kinetic parameters (average surface residence time and concentration of surface intermediates) were calculated using the method described by Shannon and Goodwin¹⁰. By integrating the normalized decay response to the step change in isotopic concentration relative to the measured gas phase hold-up, the mean surface residence time of all carbon-containing adsorbed CO₂ surface intermediates (τ_{CO_2}) was able to be determined. The concentration of surface intermediates was determined from $\tau_{CO_2} \bullet R_{CO_2}$, where R_{CO_2} is the rate of CO₂ formation. The distributions of the pseudo-first-order rate constant ($k=1/\tau_{CO_2}$) were calculated from the isotopic transients for CO₂ using the method described by Hoost and Goodwin¹². This method is based on a constrained, standard Tikhonov regularization of Fredholm integral equations of the first kind. It reveals the distribution of activity, k , for the reaction sites. This distribution is represented by $F(k)$.

4. NCSU Results and Discussion

Using catalyst characterization techniques, we are able to determine certain characteristics of the catalyst that act as a basis for explaining the difference in the performance of our supports. Our research focuses on two techniques to accomplish our goal: CO pulse chemisorption and CO TPD. The large size of our supports inhibits the feasibility to use other characterization techniques without destroying the catalyst. Currently, we are unable to cut the catalyst for fear of catalytic deposition loss. Table 4.1 shows typical results for these two characterization techniques.

<i>Data Interpretation Results</i>	<i>Pulse Chemisorption</i>	<i>TPD</i>
Number of active sites	✓	✓
Dispersion	✓	✓
Desorption temperature		✓
Average metal crystallite size	✓	✓
Activation energy	✓	✓
Kinetic rate constant	✓	✓

Table 4.1: Obtainable results from pulse chemisorption and TPD

In our case, we are not able to determine the activation energy or the kinetic rate constant of adsorption/desorption because of the lack of control of the temperature ramp rate. For our results, the dispersion and number of active sites for pulse chemisorption are more accurate than TPD because of the sensitivity of our data acquisition system and the nature of the smaller versus larger integration areas.

4.1 CO Pulse Chemisorption

4.1.1 Theory

The number of metal active sites is calculated by finding the total number of moles of adsorbate that adsorb onto the metal. In our case, the adsorbate is CO. For pulse chemisorption, this is accomplished by pulsing in known volumes of CO to the catalyst until saturation (equation E1). $P_{\text{CO,loop}}$, $V_{\text{CO,loop}}$, and $T_{\text{CO,loop}}$ are the pressure, volume, and temperature of CO in the sample loop, respectively, and R is the universal gas law constant, evaluated as $8.314 \text{ J}/(\text{mol}^\circ\text{K})$. Saturation is determined when the known amount of CO being pulsed is completely detected by the NDIR and no more CO is adsorbed by the catalyst. Typically there is a gradual increase in the peak of the pulses until it reaches a saturation point, as shown in Figure D.1 in Appendix D.

We can calculate the number of moles of CO from ppm by knowing the integrated area under the ppm versus time curve and the NDIR inlet flow rate from equation E2. $n_{\text{CO,NDIR pulse}}$ is the moles of CO per sample loop pulse, and P , T , and \dot{N}_{total} are defined as the pressure, temperature, and molar flow rate of the NDIR inlet gas stream, respectively. Neglecting the addition of gas from the sample loop, the molar NDIR inlet

flow rate correlates to the volumetric pure N₂ gas flow rate (\dot{V}_{N_2}). The integration of the ppm versus time curve is done initially using the trapezoidal rule in Microsoft Excel, and then by Matlab using a spline method and a step size of 0.001 seconds for a more accurate result. The Matlab program has the ability to input the time interval for the integration, leading to a more accurate and defined integration of the pulse curve. An example of a theoretical CO pulse is shown in Figure D.2 in Appendix D.

Assuming a 1:1 relationship for CO: Pt adsorption, once we find the number of moles of adsorbed CO, we can determine the number of moles of active Pt from equation E3. CO adsorbing onto Pt can have many different configurations, from linear (1:1) to bridged (1:2) to bidentate (2:1) bonding¹³, but the predominant bond relationship at a coverage less than 50% is the linear bond, at P = 101.325 kPa and T = 300-500 K^{14,15}. $n_{\text{metal,active}}$ is the moles of active metal saturated by CO adsorption, $n_{\text{CO,saturate}}$ is the moles of CO required to saturate the metal surface, and N_{AV} is Avogadro's number, evaluated as 6.023×10^{23} atoms/mol.

$$n_{\text{CO,loop}} = \frac{V_{\text{CO,loop}} * R * T_{\text{loop}}}{P_{\text{loop}}} \quad \text{E1}$$

$$n_{\text{CO,NDIR pulse}} = \int_0^{\infty} (\text{ppm CO}) (\dot{N}_{\text{total}}) dt = \frac{P \dot{V}_{N_2}}{RT} \int_0^{\infty} (\text{ppm CO}) dt \quad \text{E2}$$

$$n_{\text{metal,active}} = \frac{n_{\text{CO,saturate}} * N_{AV} \left(\frac{\text{CO atoms}}{\text{mol}} \right)}{N_{AV} \left(\frac{\text{Pt atoms}}{\text{mol}} \right)} \quad \text{E3}$$

The role of Fe is not completely understood in our characterization calculations. Fe, like Pt, does not always have a linear adsorbing relationship. CO can adsorb onto Fe in a linear, bridged, bidentate¹⁶, or four-fold (4:1) CO:Fe bond^{16,17}. Since we do not know the exact configuration, the Fe weight loading is relatively low compared to Pt, and the bridged configuration is unlikely because of low Fe loading, we assume a 1:1 CO:Fe adsorption to act as a lower bound for our calculations.

Typically, chemisorption and TPD of metals (excluding metal oxides and sulfides) is tested with H₂ because H₂ adsorption generally occurs by dissociation into two H atoms (1:1 H:metal relationship). This confidence allows for more consistent results¹⁸. The stoichiometry of CO adsorption on metals is highly variable because of the possibility of linear to multi-fold adsorption^{13,19}; however, since our predominant PROX reaction involves CO, we use CO as our chemisorption gas.

Metal dispersion is the ratio of the actual amount of catalytic metal that actively adsorbs CO to the total amount of catalytic metal washcoated on the support (equation E4). Dispersion gives us an idea of how much of the catalytic metal that is deposited on the support is active in adsorbing CO. A higher dispersion value equates to a more efficient

metal atom usage for catalytic reaction²⁰. For example, a catalyst with 100% dispersion has every metal atom available for adsorption.

$$\text{Dispersion (\%)} = \frac{\text{grams of CO - adsorbing metal}}{\text{total grams of catalytic metal}} * 100\% \quad \text{E4}$$

The last data interpretation for pulse chemisorption is the average metal crystallite size. The average metal crystallite size is a more accepted and manageable physical parameter which can be converted from the dispersion calculation²⁰. In order to find the diameter of the metal, one must assume a geometric model that describes the shape of the deposited metal. The formula for a spherical model is shown in equation E5²⁰.

$$d_{\text{metal}} = \frac{6}{\rho * S_g * \text{Dispersion}} \quad \text{E5}$$

Where d_{metal} is the average metal crystallite size, ρ is the density of the metal (g metal/cm³), and S_g is the maximum surface area possible per gram metal basis (cm²/g metal). Other geometric models can be used to describe the shape of the deposited metal, such as a cubic model¹³. Without knowing the actual geometry of the metal, the crystallite sizes are rough estimates of the actual size. Larger crystallite diameters indicate clumping and clusters of metal, translating into poor dispersion of the metal on the support.

Average metal crystallite sizes were not determined for chemisorption because the data is unclear as to whether it is the Pt or Fe that is chemisorbing the CO, and the calculation is dependent on the metal physical properties ρ and S_g .

4.1.2 Data Analysis

4.1.2.1 Standards

The first set of tests was done on a blank reactor with no support inside. A standard test was done to see how the NDIR detector responded to a known volume pulse of CO. If the number of moles calculated from the NDIR is less than the number of moles in the pulse, then adsorption of CO occurs in the system. If the number of moles calculated from the NDIR is the same as the number of moles in the pulse, then no adsorption of CO occurs in the system. We expect the latter to occur. From equation E1 in section 4.1.1, one can calculate the number of moles of CO per pulse ($n_{\text{CO,loop}}$), given the temperature, pressure, and volume of the sample loop.

Converting the ppm values of CO taken from the NDIR to molar values requires multiplication of the integrated area under the ppm versus time curve and the pure N₂ flow rate, as shown in equation E2 in section 4.1.1. The moles of CO in the integrated pulse ($n_{\text{CO,NDIR pulse}}$) is compared to $n_{\text{CO,loop}}$ to see if there is any difference between the two values. The NDIR is spanned with a 203 ppm CO in N₂ cylinder prior to the test. 10 pulses were done for each set of N₂ flow rates, and the average error was calculated. Initial tests show that the value of $n_{\text{CO,NDIR pulse}}$ is always higher than the value of $n_{\text{CO,loop}}$.

We take this to assume that no CO is being adsorbed by the system. The data is summarized in Table 4.2, where the associated error is defined by equation E6.

Pure N ₂ flow rate	1.0 L/min N ₂	1.5 L/min N ₂	2.0 L/min N ₂
Error	6.0%	12.4%	19.5%

Table 4.2: Blank reactor data at various N₂ flow rates

$$\text{Error} = \frac{n_{\text{CO,NDIR pulse}} - n_{\text{CO,loop}}}{n_{\text{CO,NDIR pulse}}} * 100\% \quad \text{E6}$$

The next set of initial tests was done with an uncatalysed, unwashcoated blank foam. The same tests done on the blank reactor were also done on the blank foam, and again we expected no CO adsorption to occur, except this time on the blank foam. 10 pulses were done for each set of N₂ flow rates, except for the second 1.0 L/min, 905 ppm CO in N₂ trial where only 3 were done, and the average error was calculated. The results are summarized on Table 4.3.

Span gas used (ppm CO in N ₂)	905 ppm (first try)	203 ppm	905 ppm	203 ppm	905 ppm (second try)
Pure N ₂ flow rate (L/min N ₂)	1.0 L/min	1.0 L/min	1.5 L/min	1.5 L/min	1.0 L/min
Error	9.3%	18.7%	18%	30%	8.0%

Table 4.3: Uncatalysed, unwashcoated blank foam data at various N₂ flow rates and NDIR span gas cylinders

The higher span gas has a greater accuracy towards the molar CO value in the sample loop compared to the lower span gas. Again, the value of $n_{\text{CO,NDIR pulse}}$ is always higher than the value of $n_{\text{CO,loop}}$, so we assume that no CO is being adsorbed by the blank foam.

The rest of the data is summarized in Table D.1 in Appendix D. For all runs, the value of $n_{\text{CO,NDIR pulse}}$ is always higher than the value of $n_{\text{CO,loop}}$. We make the assumption that because of this phenomenon, there is no CO uptake either by the foam support or the system. A possibility for this variation is that all our gases, supplied by National Welders, have a $\pm 2\%$ accuracy. For example, the 905 ppm CO in N₂ cylinder translates into a range of 887-923 ppm CO in N₂ for a $\pm 2\%$ accuracy. These variations affect the three distinct variable CO cylinders used 1) to span the NDIR, 2) as a pulse gas for the chemisorption, and 3) as the saturation gas for the TPD. In turn, the 10% CO in N₂ cylinder used for the pulse gas translates into a range of 9.8-10.2% CO in N₂, which changes the values for $n_{\text{CO,loop}}$ and affects the error calculated in equation E6.

Another note is the magnitude of error should not be flow rate dependent since the same amount of CO is being pulsed into the reactor. The data indicates that for a higher flow rate of 1.5 L/min pure N₂, the error is greater than for 1.0 L/min pure N₂. One explanation for this is that the CO analyzer for the NDIR is dependent on the flow rate.

The range of flow rates for the NDIR to be accurate is 0.5-2.0 L/min per component. One way to test this explanation is to use the 905 ppm CO in N₂ span gas cylinder at various flow rates from 0.5 to 2.0 L/min and observe for any changes in the CO reading at higher flow rates.

Another reason for this may be that the pure N₂ flow rate from the mass flow controller control and readout equipment is not accurate, affecting the value of $n_{CO,NDIR\ pulse}$. The control and readout equipment would not only have to be incorrect, but also nonlinear at higher flowrates to account for the greater magnitude of error at higher flow rates. Two ways of testing this theory is to use a wet test meter, and/or a soap bubble flow meter to check the flow rate of the pure N₂ mass flow controller.

4.1.2.2 'Identical' Supports

Three nominally 'identical' pieces of support were placed together to test the activity and selectivity of the supports, either metal foams or ceramic monoliths, at varying linear velocities and GHSVs, as described in section 1.2. Variations were noted in their individual activity and selectivity, as shown on Figure 1.2. The one "older" piece was more active and selective than the two "newer" pieces of support. We use pulse chemisorption to help determine the causes for these differences. At present, none of the 'identical' ceramic monoliths have been tested, and only two of the 'identical' metal foams have been tested.

For the 5 wt% Pt, 0.5 wt% Fe, 40 ppi, 4% ρ metal foams that were tested, there was no significant difference in the number of active metal or metal dispersion. Summarized data can be found on Table 4.4. The nominal weight loading approximated 5.05 wt% active metal (both Pt plus Fe), but chemisorption reveals a much lower active metal value. These results do not indicate a reason for the difference in activity and selectivity seen in the individual pieces. Comprehensive information on the tests is found on Table D.2 in Appendix D.

Metal Foam Pieces	trial	Active Metal	Metal Dispersion
one of two "newer" pieces of metal foam	one	0.277-0.287%	5.04-5.22%
	two	0.360-0.367%	6.55-6.67%
"older" piece metal foam	one	0.240-0.247%	4.37-4.50%
	two	0.330-0.332%	6.00-6.04%

Table 4.4: Chemisorption 'identical' pieces of metal foam intracomparison

In Figure D.2, a typical theoretical pulse of CO is shown, which is close to symmetrical around the peak. Tests done on the uncatalysed, unwashcoated blank foam and blank reactor have pulses that simulate this typical pulse. As shown on Figure D.1, there are three stages that characterize pulse chemisorption:

- 1) complete CO uptake, where no CO is detected in the outlet (pulses 0-1)
- 2) partial CO uptake, where the CO peak maximum increases each pulse (pulses 2-5)
- 3) no CO uptake, where all the CO pulsed is detected in the outlet (pulses 6-8)

Alternatively, tests done on our supports with active metal washcoated on them show a different shape. The first stage where complete CO uptake occurs is observed. In the second stage, an elongated tail is seen towards the end of the pulse, often lasting longer than 10 minutes and not dropping to 0 ppm CO. A graphical representation is shown on Figure D.3 in Appendix D. In the third stage, no CO uptake occurs, but the value of $n_{\text{CO,NDIR pulse}}$ is much greater than $n_{\text{CO,loop}}$, often times with an error greater than 20%. An example of an elongated tail pulse is shown on Figure D.4 in Appendix D.

Two possibilities can explain the elongated tail. The first possibility is that the Fe is weakly chemisorbing multiple CO. Korotkikh and Farrauto originally observed that Pt/Al₂O₃ promoted with a metal oxide, with no inlet CO₂, had a much higher activity and selectivity than unpromoted Pt/Al₂O₃⁶. In a later article, Liu et al mention that Fe is the promoted metal on Pt/Al₂O₃, and that when Fe is deposited it prefers the Pt instead of the Al₂O₃. Since Fe is positioned on the surface of the Pt, it partially covers the surface and lowers the amount of CO adsorption⁷. Liu et al also mentions that Fe can weakly adsorb CO. Similar results were found on hydrocarbon conversion at stoichiometric conditions; after an O₂-H₂ treatment, Fe dissolves into the Pt lattice²¹. As mentioned in section 4.1.1, the role of Fe is not understood in our calculations, but it can adsorb CO up to a four-fold bond, which blocks CO adsorption by Pt if Fe decorates its surface. Farrauto and Bartholomew mention that iron carbonyl, Fe(CO)₅, can form at moderate to room temperatures (273-573 K)¹⁸ and volatilize off the support^{18, 22}. Since Fe weakly adsorbs CO, it may be desorbing slowly and creating the elongated tail.

We hypothesized that if there was no Fe, we would not see an elongated tail. To test this theory, we used pulse chemisorption on a 400 cpsi, 5 wt% Pt with no Fe to see if a tail developed. The results show that a tail did develop, similar to Figure D.4, and that we reached 25-30% over the value of $n_{\text{CO, loop}}$.

The second possibility is that the γ -Al₂O₃ washcoat and surface impurities are physisorbing CO and causing it to slowly bleed out of the system. The exact catalyst preparation procedure used by Environex is unknown, but binding agents and other chemicals which are typically used may physisorb CO and cause the bleed out.

The task to differentiate whether the γ -Al₂O₃ washcoat, Fe, or both, is adsorbing the CO is difficult. We will retest catalysts, with and without the presence of Fe, the next day after saturation by chemisorption the day prior to see if there is any more uptake of CO. If there is no uptake of CO the next day, after saturation the day prior, by the catalyst with no Fe, but uptake of CO by the Fe-promoted catalyst, then it is the Fe that is the cause of the elongated tail. If uptake of CO occurs on both the Fe-promoted and non-Fe catalysts, then it is the γ -Al₂O₃ washcoat causing the elongated tail.

4.1.2.3 Varying ppi and ρ Metal Foams

Figure 1.1 in section 1.2 depicts the activity and selectivity of 5 wt% Pt, 0.5 wt% Fe, various ppi and ρ metal foams. As mentioned in section 1.1 above, the most active and

selective metal foam was the 40 ppi, 4% ρ , while the 40 ppi, 12% ρ was the least active and selective. We use pulse chemisorption to help understand these differences.

At this point, only the 40 ppi, 4% ρ and the 20 ppi, 12% ρ have been tested. The results are summarized on Table 4.5 below. The first three trials of the 20 ppi, 12% ρ foam had the gas chiller unplugged to try to keep a consistent temperature when zeroing and spanning the NDIR. The zero gas went through the gas chiller, but the span gas did not. Comprehensive information on the tests is found on Table D.3 in Appendix D.

Metal Foam Pieces	trial	Active Metal	Metal Dispersion
40 ppi, 4% ρ “older” piece	one	0.240-0.247%	4.37-4.50%
	two	0.330-0.332%	6.00-6.04%
20 ppi, 12% ρ	one	0.835-0.847%	15.2-15.4%
	two	0.424-0.430%	7.71-7.82%
	three	0.602-0.575%	10.9-10.5%
	four	0.549-0.552%	9.99-10.0%

Table 4.5: Chemisorption comparison of 5 wt% Pt / 0.5 wt% Fe, varying ppi and ρ metal foams

Of the results collected, one expects the 40 ppi, 4% ρ metal foam to have the higher metal dispersion and active metal count because it has the highest CO activity and selectivity. Instead, the 20 ppi, 12% ρ has both higher active metal count and metal dispersion. One theory is that the Fe loading on the 20 ppi, 12% ρ is either lower than 0.5 wt%, or less Fe is exposed on the surface. A higher Fe presence on the surface inhibits CO adsorption on Pt; Liu et al observes that Fe-promoted Pt/ γ -Al₂O₃ reaches only 75% of non-promoted Pt/ γ -Al₂O₃ CO uptake⁷. The higher Fe presence would explain the higher activity and selectivity, and lower metal dispersion and active metal count, of the 40 ppi, 4% ρ metal foam. A more complete data set is needed for an accurate analysis of distinguishing characteristics of the varying ppi and ρ metal foams.

For the 40 ppi, 4% ρ metal foam, the active metal count and metal dispersion for the two trials do not differ greatly. For the 20 ppi, 12% ρ metal foam, the active metal count and metal dispersion vary as much as 200%. The first trial had a high CO adsorption, yielding 15% dispersion, but the second trial had a lower CO adsorption, yielding only 7-8% dispersion. The third and fourth trials had intermediate CO adsorptions, yielding 10-11% dispersion. It is inconclusive why the same catalytic support yielded different values in each trial.

4.1.2.4 Varying Fe Ceramic Monoliths

Figure 1.3 in section 1.2 depicts the activity and selectivity of a 5 wt% Pt, varying Fe loading ceramic monolith at T_{in} =100°C and 170°C. To help explain the role of Fe promotion on Pt on its activity and selectivity, we use pulse chemisorption. Previous literature from Korotkikh and Farrauto, Liu et al, and Sakamoto et al describe the activity

and selectivity of Fe-promoted on Pt and how Fe integrates onto the Pt surface^{7, 18, 21}. An extensive explanation is found above in section 4.1.2.2.

Ceramic Monolith Pieces	Active Metal	Metal Dispersion
0.05 wt% Fe	0.275%	5.44-5.45%
0.0 wt% Fe	0.338-0.349%	6.75-6.98%

Table 4.6: Chemisorption comparison of 400 cpsi, 5 wt% Pt, varying Fe ceramic monoliths

The results are summarized on Table 4.6. At this point, only the 0.0 wt% and 0.05 wt% Fe have been tested. Since Fe is assumed to be found near the Pt surface, it should inhibit CO adsorption onto the Pt surface and lower the metal dispersion and active metal count. Comprehensive information on the tests is found on Table D.4 in Appendix D. The current data follows the trend of higher dispersion and active metal count at lower Fe loadings, but a more complete data set is needed for an accurate analysis of the role of Fe on the activity and selectivity of the ceramic monoliths.

4.2 CO Temperature Programmed Desorption

4.2.1 Theory

Similarly to pulse chemisorption, TPD can be used to determine the metal dispersion, active metal count, and the average metal crystallite size. The equations behind these calculations can be found in the pulse chemisorption theory in section 4.1.1. We assume that our TPD results reflect only Pt adsorption, while our pulse chemisorption assumes both Pt and Fe adsorption. We justify this assumption because we flood the catalyst the day prior to the TPD run, and allow physisorbed and weakly chemisorbed CO to bleed off the support overnight. We also presume that any CO adsorbed onto the Fe, γ -Al₂O₃ washcoat, or both, falls into these categories, leaving only chemisorbed CO on Pt when the TPD is run the next day.

In addition to these data, our system utilizes TPD to determine the desorption temperature. From a graphical analysis of the TPD data, the CO desorption temperature can be determined by the location of the CO peak. Often times the strength of the CO-metal bond is associated with its' desorption temperature: the higher the desorption temperature, the stronger the bond and adsorption site. This desorption temperature is often reported as the general temperature that CO desorbs off the metal. For CO adsorbed on Pt, the desorption temperature peaks $\sim 160^{\circ}\text{C}$ ⁴. A typical graphical representation of TPD data is shown on Figure E.1 on Appendix E.

The desorption temperature acquired from TPD data may be misleading. The desorption temperature is dependent on the porosity of the catalyst and its support^{13, 14}, the linear temperature ramp rate, and the inert gas flow rate²³. The faster the linear ramp rate, the higher the desorption temperature value. If the catalyst or its support is porous, readsorption of CO onto another metal after it has desorbed is a strong possibility. This effect shifts the maximum of the desorption temperature peak to a higher temperature because CO diffusion to the detector requires a longer period of time. The slower the gas

inert flow rate, the greater the lag time from the desorption of CO to the detector, increasing the desorption temperature value. Compounding these three effects of a fast linear ramp rate, multiple readsorption sites, and lag time for a slow inert flow rate, the TPD desorption temperature peak may not reflect its actual value.

4.2.2 Data Analysis

4.2.2.1 Standards

The same tests completed on the unwashcoated, uncatalysed blank foam and the blank reactor for pulse chemisorption are used for TPD. The results and analysis is found above under section 4.1.2.1. No TPD was completed on the blank foam or blank reactor because the pulse chemisorption data revealed no CO adsorption.

4.2.2.2 'Identical' Supports

None of the 'identical' ceramic monoliths have been tested yet, and only the second trial of the "older," more active and selective 40 ppi, 4% ρ 'identical' metal foam was tested with TPD. Using a ramp rate of 2-3°C/min, the active Pt was 0.23%, or a 4.7% Pt dispersion. The calculated average Pt crystallite size (d_{Pt}) from equation E5 in section 4.1.1 was 260 Å (26 nm). The desorption temperature (T_{des}) was 145°C. Comprehensive information on this test is found on Table E.1 in Appendix E.

The TPD results for active metal count and dispersion are lower than the results from pulse chemisorption, 0.23-0.33% and 4.5-6.0%, respectively, from Table 4.4. We expect the TPD results to be lower than the pulse chemisorption because the TPD results measure only CO adsorption on Pt, explained in section 4.2.1. On the other hand, pulse chemisorption data measures CO both chemisorbed on Pt, and either physisorbed or weakly chemisorbed on Fe, resulting in higher values.

For Fe-promoted Pt/ γ -Al₂O₃ catalysts, Liu et al used TEM and HRTEM to discover dispersed Pt particles with an average size of ~2 nm⁷. Sakamoto et al determined the average Pt particle size to be ~20 nm using both XRD and dark field TEM²¹. The results of both Liu and Sakamoto yielded d_{Pt} values that were much lower than the values calculated using our results. It is possible that our assumption of a spherical-shaped geometric model is incorrect, or significant sintering by agglomeration of the Pt particles occurs, especially in the presence of water vapor¹⁸. Conversely, Sakamoto postulates that one of the roles of Fe is to create a layer of Fe₂O₃ to prevent Pt sintering²¹, which concurs with Farrauto and Bartholomew, who also mention that pores and support surface defects impede surface migration of metal particles¹⁸. A cubic geometric model from White, or a combination of a spherical model with flat sides may provide smaller d_{Pt} values¹³.

4.2.2.3 Varying ppi and ρ Metal Foams

TPD results on the varying ppi and ρ metal foams do not show significant differences in the active Pt, Pt dispersion, or d_{Pt} . These results are summarized on Table 4.7. The high values for d_{Pt} analysis explained in section 4.2.2.2 is applicable to this data set. The TPD results ranked from highest to lowest are:

40 ppi, 12% ρ > 20 ppi, 12% ρ (trial four) [> 20 ppi, 4% ρ] > 40 ppi, 4% ρ

For the 20 ppi, 12% ρ metal foam, trial four is chosen because it was the only run with the gas chiller plugged in, as described in the comprehensive information section found on Table E.3 in Appendix E. The 20 ppi, 4% ρ metal foam was not tested, but we believe that this support would fall in the given location. The order of these results is the exact reverse of their activity and selectivity results, ranked from highest to lowest, as shown in section 1.1. As discussed in the pulse chemisorption results in section 4.1.2.3, the 12% ρ metal foams may have less than the stated 0.5 wt% Fe content, leading to a reduced blocking of Pt sites and a higher CO adsorption, as stated by Liu et al⁷ and Sakamoto et al²¹, than the 4% ρ metal foams.

Metal Foam Pieces	trial	Active Pt	Pt Dispersion	d_{Pt}	T_{des}
40 ppi, 4% ρ "older" piece	two	0.232-0.235%	4.65-4.69%	260-258 Å	145°C
20 ppi, 12% ρ	one	<i>Total (spline):</i> 5.03%	<i>Total (spline):</i> 101%	<i>Total (spline):</i> 12 Å	145°C 300°C
	two	0.243-0.245%	4.87-4.90%	247-249 Å	155°C
	three	0.536-0.538%	10.7%	113 Å	178°C
	four	0.275-0.285%	5.50-5.69%	220-213 Å	155°C
40 ppi, 12% ρ	--	0.453-0.460%	8.24-8.36%	147-145 Å	113- 128°C

Table 4.7: TPD comparison of 5 wt% Pt / 0.5 wt% Fe, varying ppi and ρ metal foams

The 40 ppi, 12% ρ metal foam has a range for T_{des} because of incongruent heating between the inlet and outlet of the reactor, causing a temperature profile. According to Manasilp and Gulari, the desorption temperature for CO on Pt is $\sim 160^\circ\text{C}$ ⁴. Our T_{des} data generally falls $\sim 160^\circ\text{C}$, both below and above the value. As explained in section 4.2.1, multiple variables affect the temperature at which CO desorbs from CO. The catalytic supports are very porous, and readsorption of CO on another Pt surface is possible, increasing the time it takes for CO to reach the NDIR^{13, 14}. Keeping a constant linear ramp rate is difficult because the heating unit for TPD consists of 13 different heating tapes with various heating rates. Our linear ramp rates are $\sim 2\text{-}5^\circ\text{C}/\text{min}$, which is at the lower end for TPD experiments. A lower linear ramp rate will decrease T_{des} . The pure N_2 flow rate of 1.0 L/min may be fast, decreasing the lag time between the reactor and the NDIR, which decreases T_{des} ²³.

The TPD results, compared to the pulse chemisorption results on Table 4.5, are significantly different. For the 40 ppi, 4% ρ and 20 ppi, 12% ρ , trials two and four, metal foams, the pulse chemisorption results were higher than the TPD results, which is expected because we assume TPD only measures CO adsorption on Pt, while pulse chemisorption measures on both Pt and Fe. A detailed explanation can be found in sections 4.2.2.2 and 4.2.1. On TPD trial three for the 20 ppi, 12% ρ metal foam, the NDIR did not drop down to 0 ppm CO after 3 hours, but baselined at 4-5 ppm, which caused the higher values. Neglecting the baseline tail on trial three, the active Pt count,

Pt dispersion, and d_{Pt} drops to 0.396%, 7.91%, and 153 Å, respectively. These values neglecting the baseline tail follow the lower TPD results trend seen on trials two and four.

The first TPD trial on the 20 ppi, 12% ρ metal foam produced a bimodal peak, shown on Figure E.2 in Appendix E. The T_{des} of the first CO peak occurs at 145°C, which concurs with the other metal foams and is within range of ~160°C⁴. The T_{des} of the second CO peak occurs at 300°C. The results are summarized on Table 4.8.

If you sum up the active Pt count and Pt dispersion, you calculate 5.03 wt%, and 101%, respectively. It is currently unknown if this is a coincidence, or if all 5 wt% Pt adsorbed CO, leading to 100% dispersion. Combining both peaks, the d_{Pt} was calculated to be 12 Å (1.2 nm), which correlates more with the results of Liu et al of 2 nm Pt particles⁷ and Sakamoto et al of ~20 nm²¹. Comparatively, the pulse chemisorption results for this trial yielded much higher dispersion values than any other metal foam runs. Three other TPD trials were run, but the results from trial one were irreproducible, similarly to the pulse chemisorption data described in section 4.1.2.3. It is inconclusive as to why the same catalytic support yielded different values in each trial.

Metal Foam Piece	Peak	Active Pt	Pt Dispersion	d_{Pt}	T_{des}
20 ppi, 12% ρ Trial One	one	0.336%	6.71%	180 Å	145°C
	two	4.70%	93.9%	13 Å	300°C
	Total Peaks (spline method)	5.03%	101%	12 Å	--

Table 4.8: TPD bimodal peak results for the 20 ppi, 12% ρ metal foam, trial one

4.2.2.4 Varying Fe Ceramic Monoliths

Only the 5 wt% Pt, 0 wt% Fe ceramic monolith was tested using TPD. Using a ramp rate of ~2.5°C/min, the active Pt was 0.23%, the Pt dispersion was 4.6%, the d_{Pt} was 260 Å (26 nm), and T_{des} was 136°C. Comprehensive information on this test is found on Table E.2 in Appendix E. The results for this ceramic monolith were similar to the TPD results for the “older” 40 ppi, 4% ρ metal foam discussed in section 4.2.2.2, hence the analysis for the high d_{Pt} value compared to Liu et al⁷ and Sakamoto et al²¹ is applicable.

The TPD results for active metal count and dispersion are lower than the results from pulse chemisorption, 0.34% and 6.8%, respectively. As hypothesized previously in section 4.1.2.2, physisorption of CO can bond weakly to the γ -Al₂O₃ washcoat or surface impurities, leading to higher values for pulse chemisorption data compared to TPD. A complete data set is needed for an accurate analysis of the role of Fe on the activity and selectivity of the ceramic monoliths.

5. Clemson Results and Discussion

5.1 Catalyst Characterization

As shown in Table C.1 in Appendix C, Fe addition did not change the BET surface area of the catalysts. It was approximately $230 \text{ m}^2/\text{g}_{\text{cat}}$ for both Pt and PtFe catalysts.

The amounts of hydrogen and carbon monoxide irreversibly chemisorbed on the Pt and PtFe catalysts and the % metal dispersions are shown in Table C.1. The average metal particle sizes were ca. 4.5 nm for the PtFe catalyst and 2.4 nm for the Pt one. These quantities were calculated based on the irreversible hydrogen chemisorption and the correlation between % dispersion and metal particle size as described by Anderson²⁴.

It is obvious from Table C.1 that the amounts of CO and H₂ chemisorption on the PtFe catalyst were lower than on the Pt one. The amount of irreversible CO chemisorbed on the PtFe catalyst was only 61% that on the Pt one while the amount of irreversible H₂ chemisorption was ca. 71%.

5.2 Temperature Programmed Reduction

Reduction behaviors of alumina-supported Pt, PtFe, and Fe catalysts obtained by TPR experiments are shown in Figure C.1 in Appendix C. The Pt catalyst showed only one reduction peak at $\sim 218^\circ\text{C}$. Two reduction peaks were observed for the PtFe catalyst, as expected. The first peak represents platinum oxide reduction and perhaps some catalytic reduction of iron. The second peak at $\sim 290^\circ\text{C}$ is the catalytic reduction of iron oxide. Comparing these results to the results for an Fe/ $\gamma\text{-Al}_2\text{O}_3$ catalyst that exhibited 2 reduction peaks at 377 and 464°C , it is obvious that Pt decreases the reduction temperature required for iron oxide as a result of hydrogen spillover. While Jia et al.²⁵ reported some higher temperature peaks for Pt/ $\gamma\text{-Al}_2\text{O}_3$, the present results are consistent with most previous works on Pt²⁶⁻²⁸. Based on the data, the reducibility of the Pt catalyst was 100% with negligible reduction at temperatures lower than 40°C .

5.3 Temperature Programmed Desorption

Figure C.2 in Appendix C shows the TPD profiles of H₂, CH₄, CO and CO₂ for desorption of the adsorbed gas mixture (1% CO, 45% H₂ in He). Both Pt and PtFe gave similar desorption behavior except for methane, where the peak was shifted slightly. Surprisingly, no peak for the desorption of CO was observed for any of the catalysts, but there was a peak for CO₂ desorption at ca. 320°C for Pt and PtFe, and at ca. 180°C for Fe, indicating the higher activity of Fe for the Boudourd reaction. There was a broad peak for H₂ desorption starting at 220°C with a peak around 600°C that was essentially identical for Pt, PtFe, and Fe. No low temperature peak for H₂ desorption was observed as reported by Miller et al.²⁹ for TPD of pure hydrogen adsorbed on Pt/ $\gamma\text{-Al}_2\text{O}_3$. Since the H₂ peak was very broad starting at 220°C , it is possible that some desorption occurred at lower temperature and contributed to the background.

5.4 Activity Measurement

The PtFe catalyst was tested for its activity and selectivity and compared to that for the non-promoted Pt catalyst. The space velocity used was four times that used for the non-promoted catalyst in order to have differential conversion at steady state. Assuming that oxygen is consumed by either CO or H₂ oxidation, the rate of H₂ oxidation can be calculated. Rates of CO, H₂ oxidation and %CO₂ selectivities of the PtFe and Pt catalysts with time-on-stream (TOS) are plotted together for comparison purposes in Figure C.3 in Appendix C. The CO oxidation rates of both catalysts dropped significantly with TOS. An increase in H₂ oxidation rate was detected for Pt reflecting the decrease in %CO₂ selectivity. Although rate of H₂ oxidation increased with TOS, it was not significant compared to the rapid decrease in rate of CO oxidation resulting in the rapid decrease in total oxidation rate. PtFe showed an opposite change in H₂ oxidation rate. Decrease in H₂ oxidation rate along with CO oxidation rate resulted in a slower decrease in %CO₂ selectivity. The Fe-promoted catalyst reached a pseudo steady-state after 300 min time-on-stream whereas the non-promoted catalyst reached steady-state after only 30 min. However, considering the relative change in activity to steady state, both catalysts would appear to have had the same degree (%) of deactivation. The initial CO oxidation rate on PtFe was about 5.7 times higher than that on unpromoted Pt (48.2 vs. 8.3 μmole/g_{cat}/s). At steady-state, this ratio was slightly lower (~ 4). The CO₂ selectivity on PtFe was also higher than that on Pt during most of the TOS. At steady-state, Pt gave 27% CO₂ selectivity whereas PtFe gave almost 50%. An initial reproducible slight increase in selectivity during 5-10 min TOS was observed for PtFe.

Additional experiments were performed to determine the effect of oxygen and carbon monoxide partial pressure on the reaction rate and selectivity as shown in Table C.2 in Appendix C. The partial pressures of oxygen and carbon monoxide were varied between 0.9 kPa and 3.6 kPa. The process parameter, λ , is defined as two times the ratio of partial pressures of oxygen and carbon monoxide. If keeping $\lambda=2$ ($P_{CO}=P_O$), partial pressure of CO had a positive effect on the CO oxidation rate (both initial and steady state) for both Pt and PtFe. A surprising result is the effect of oxygen partial pressure. It affected the initial reaction rate for both Pt and PtFe but with TOS, its effect became greater for Pt but became less and less for PtFe, being negligible at steady state. Selectivity was also affected by changing the partial pressures of the reactants. For Pt, even though there was no clear direct dependence of the initial selectivity on CO partial pressure, the steady-state selectivity may have increased slightly with P_{CO} . For PtFe, both initial and steady-state selectivity increased with P_{CO} . There was no clear evidence of oxygen partial pressure dependency of selectivity for either Pt or PtFe.

The power law expression for CO oxidation on both catalysts was determined. The approach we used has been described by Kahlich et al.⁹. At $\lambda=2$ and steady state operation, the reaction orders for the power law form of the rate expression for Pt were found to be +1 and 0 for O₂ and CO, respectively. The PtFe catalyst had reaction orders of 0 and 0.2 for O₂ and CO, respectively. This change in reaction order for O₂ indicates the impact of Fe promotion on the mechanism or at least the surface adsorption parameters.

To better understand the cause of catalyst deactivation, additional experiments were performed by pre-exposing the reduced catalyst to a stream of O₂/He or CO/He at reaction temperature (90°C) for 1 h before starting the reaction. The results are shown in Figure C.4 in Appendix C. Initial reaction rate for PtFe after switching from O₂/He to the reactant stream was 44% lower than that for normal reaction and the reaction rate continued to be lower for the rest of TOS. On the other hand, contacting PtFe with CO/He before reaction had only a slight effect on the reaction rate. In contrast to PtFe, exposure of Pt to O₂/He before reaction did not have any effect on the reaction rate, but exposure to CO/He, on the other hand, decreased the initial reaction rate to the same value as at steady-state. The results from this investigation suggest that contacting PtFe with O₂ effectively deactivated it. Pre-oxidizing of Pt has little impact because Pt is quickly reduced under reaction conditions where there is a large excess of H₂. Fe in PtFe, on the other hand, is more difficult to reduce. The low activity of PtFe after pre-oxidizing the surface suggests that deactivation during reaction may be due, at least in part, to oxidation of the Fe.

5.5 Isotopic Transient Kinetic Analysis

A typical normalized transient response detected after switching from ¹²CO to ¹³CO is in Figure C.5 in Appendix C. Results from the ITKA study (Figure C.6 in Appendix C) show decreases for both Pt and PtFe in the pseudo-first-order intrinsic rate constant ($k=1/\tau_{I-CO_2}$) and concentration of surface CO₂ intermediates (N_{I-CO_2}) with TOS. Since $rate = (1/\tau_{I-CO_2}) \cdot N_{I-CO_2} = k \cdot N_{I-CO_2}$ and $k = rate/N_{I-CO_2}$, k (or $1/\tau_{I-CO_2}$), the pseudo-first order rate constant with units of reciprocal seconds, represents a measure of site TOF. At the beginning of reaction on Pt, k was 0.15 s⁻¹, decreasing to ~ 0.1 s⁻¹ after 10 min TOS and then remaining essentially constant. Fe-promotion of Pt resulted in a very high initial (5 min TOS) activity ($k \sim 1.5$ s⁻¹) but decreased by ca. 66% by 10 min TOS and continued to gradually decrease after that. The pseudo-steady-state k was 0.2 s⁻¹ for PtFe, double that for Pt. The concentration of surface intermediates also monotonically decreased with TOS for both catalysts except during the first 10 min for PtFe. The concentration of intermediates on PtFe appeared to go through a maximum between 5-10 min TOS. For the Pt catalyst, N_{I-CO_2} decreased monotonically from 57 μmole/g_{cat} down to ca. 10 μmole/g_{cat}; whereas, N_{I-CO_2} for PtFe showed an increase from 5 min TOS (~ 32 μmole/g_{cat}) to 10 min (~50 μmole/g_{cat}) and then decreased until reaching steady state (~ 20 μmole/g_{cat}). The maximum values of N_{I-CO_2} for both catalysts were essentially the same (50-57 μmole/g_{cat}).

5.6 Characteristics of the Catalyst Surface at Steady State

A stream of 50% hydrogen in helium was fed through the bed of the partially deactivated catalyst after it reached steady state reaction while the temperature in the reactor was raised from the reaction temperature to 550°C. A mass spectrometer was used to detect the composition of the effluent from the reactor. The amounts of carbon calculated from the amount of methane formed were found to be 125 and 103 μmole/g_{cat} for Pt and PtFe,

respectively. It is worth noting that this amount is very small compared to the total flow of CO during 5 min of reaction (4,200-17,400 $\mu\text{mole C/g}_{\text{cat}}$); therefore, the lack of accounting for this carbon deposition had little effect on the reported CO oxidation rate. This measurement of deposited carbon has been found to replicate that obtained by elemental analysis for carbon⁵. Figure C.7 in Appendix C shows how the carbon or coke deposition on the Pt and PtFe catalysts changed with TOS. It was found to increase significantly during the first 5 min of reaction with only a small increase over the following period.

5.7 Chemisorption and TPD Results

The chemisorption results are in agreement with the DRIFTS results for H₂ and CO adsorption obtained by Liu et al.⁷. The H₂ and CO uptakes decreased upon Fe promotion in both cases. Liu et al. concluded that partial blockage of Pt as a result of Fe decoration caused this decrease.

Considering the TPD profiles of Pt, PtFe and Fe (Figure C.2), all desorption peaks for Pt and PtFe are identical. However, although PtFe showed a similar desorption pattern as Fe for H₂, the desorption of CO₂ occurred at a much higher temperature. It is clear from the TPD results that PtFe behaved essentially like the Pt catalyst and seemed to exhibit little characteristic of an Fe surface. Fe may associate strongly with Pt or form an intermetallic compound. Considering the composition of this PtFe catalyst and the phase diagram of PtFe³⁰, it is likely that the intermetallic compound FePt₃ formed at this composition (74% atomic percent of Pt), at least to some degree. Even though the formation of the intermetallic compound is likely, during deactivation FePt₃ may have been destroyed as a result of oxidation of Fe.

5.8 Effect on Fe Promotion on Overall Activity

It is obvious that the PtFe catalyst had a superior activity and selectivity for selective CO oxidation compared to Pt. As has previously been shown⁶, PtFe is 5-7 times more active than Pt at 90°C depending on the O₂/CO ratio. However, although Korotkikh and Farrauto⁶ found no change in selectivity upon Fe promotion of Pt, we found significant improvement. Farrauto and co-workers^{6, 7} hypothesized that the promoted catalyst is more active for CO oxidation due to iron oxide providing more favorable sites for oxygen adsorption than Pt itself and being located in close contact with surface Pt. Thus, oxygen would have a greater probability for adsorption on PtFe than on Pt. Initial high oxidation rates for CO and H₂ on PtFe compared to that on Pt (Figure C.3), thus, is consistent with an increase in oxygen activation upon Fe addition. This idea also fits the results from ITKA as shown in Figure C.6a. An increase in site TOF ($k=1/\tau$) for PtFe means that reactants spend less time on the PtFe surface to produce CO₂. If molecular adsorption of oxygen is the rate-determining step in CO oxidation as previously suggested^{30, 31}, increasing the number of oxygen adsorption sites and possibly its rate would increase the overall rate of reaction and, perhaps, change the rate-determining step.

With Fe promotion, there is a significant change in reaction order in the power law rate expressions (Pt: 1 and 0, PtFe: 0 and 0.2 for O₂ and CO, respectively). On the Pt catalyst surface, it would appear that oxygen adsorption may be rate controlling as previously suggested. Reaction rate depends on oxygen adsorption since it has to compete with CO for the adsorption sites. For the case of PtFe, on the other hand, oxygen has more preferable adsorption sites on Fe. Consequently, rate has little or no dependence on oxygen partial pressures. We speculate that even at low partial pressures of oxygen and CO, i.e. 0.9 kPa, surface Fe is saturated with oxygen while surface Pt is almost saturated with CO. The power rate law for PtFe depends somewhat (0.2 power) on the partial pressure of CO, suggesting a shift in the rate- determining step.

Even though, as seen in Figure C.6b, PtFe had a higher concentration of surface intermediates during most TOS, the maximum concentration, which shows the highest possible number of active sites, was about the same as that for Pt. Despite the fact that N_{I-CO_2} of PtFe decreased with TOS at a remarkably slower rate, we can conclude that Fe promotion does not increase the maximum concentration of active sites adsorbing CO for CO₂ formation. It is important to note that N_{I-CO_2} includes only intermediates containing carbon since the isotopic tracing is done with ¹²C/¹³C. Thus, these results suggest that Fe does not promote the catalyst by providing more sites for adsorption and reaction of CO.

From a typical normalized transient response as shown in Figure C.5, the distribution of the pseudo-first-order rate constant ($k=1/\tau_{I-CO_2}$) can be calculated. The evolution of the distribution of the pseudo-first-order rate constant, representing the site activity of PtFe, with TOS is shown in Figure C.8 in Appendix C. $F(k)$ is the activity distribution for the active CO₂ intermediates on the catalyst surface. The under curve area integrated from 0 to ∞ ($\int_0^\infty F(k)dk$) is equal to 1 in all cases. Figure C.8a shows that the relative amounts of less active sites to more active sites increased as the reaction progressed, causing the mean value for the distribution to shift to a lower value of k . This suggests that deactivation occurred preferentially for the more active sites PtFe. Note that “active site” does not necessarily mean a single metal atom but may be a Pt-Fe pair. In Figure C.8b the same data was replotted after rescaling to reflect the total number of surface CO₂ intermediates and the activity of each site. The area under a curve from k_1 to k_2 corresponds to the fraction of the rate of reaction catalyzed by the active sites having activities between k_1 and k_2 . Total area for a curve corresponds to the reaction rate at that time-on-stream. It is obvious that at 30 min TOS, active sites with activities up to 0.35 s⁻¹ contributed to the reaction. As time increased, highly active sites participated less and less in the reaction. Figure C.9 in Appendix C shows the distributions of the pseudo-first order rate constant for PtFe and for Pt compared at 5-min TOS (Figure C.9a) and at steady state (Figure C.9b). As shown in Figure C.9a, initially there were a significant number of PtFe active sites that were more active than those of Pt. This portion decreased as TOS increased, as seen in Figure C.9b. The average site activity of the PtFe catalyst and the site activity distribution would appear to be asymptotically approaching that of the Pt catalyst with TOS.

5.9 Selectivity

The CO₂ selectivity with TOS both on Pt and PtFe followed the same trend as N_{I-CO_2} . For Pt, it monotonically decreased, whereas for PtFe it monotonically decreased after a small initial increase with TOS. For Pt, the large decrease in CO oxidation rate and the smaller increase in H₂ oxidation rate (Figure C.3) with TOS resulted in a rapid decrease in %CO₂ selectivity. These results suggest a change in adsorption ability of CO relative to H₂ with TOS in addition to a decrease in oxidation ability with deactivation. On the other hand, for PtFe, the decrease in both CO and H₂ oxidation rate implies that the oxidation ability of the catalyst for both reactions decreased rapidly with TOS.

5.10 Deactivation Behavior

Pt and PtFe showed different deactivation behavior considering the intrinsic site activity, k , and the concentration of active intermediates, N_{I-CO_2} . As deactivation progressed, the intrinsic site activity of Pt remained relatively constant, whereas, for PtFe it decreased significantly. On the other hand, the concentration of active intermediates for Pt decreased more rapidly with TOS compared to that for PtFe. With TOS, the site activity of PtFe appeared to asymptotically approach that of Pt indicating that its surface was becoming more like that of Pt with significant deactivation.

For both Pt and PtFe the number of active intermediates, N_{I-CO_2} , decreased significantly with TOS, although much slower for PtFe. It is likely that deactivation of Pt is simply due to carbon deposition on the surface, resulting in site blockage. On the other hand, deactivation of PtFe is due to both site blockage by carbon and some other mechanism causing a decrease in site activity, most probably related to a change in oxygen adsorption ability. Since the site activity of PtFe approached that of Pt with TOS, we suggest that deactivation decreased the promoting effect of Fe. There are many possible causes such as carbon deposition, reoxidation of Fe, and permanent deactivation such as phase separation and sintering. Since the catalysts could be regenerated by reducing in a H₂ stream, it is highly unlikely that phase separation or sintering occurred.

On the Pt catalyst the amount of carbon deposition (Figure C.7) increased significantly during the first 5 min TOS and continued to increase but at much slower rate until it exceeded the equivalent of ca. 100% surface coverage at about 200 min TOS. Since Pt still had some activity at this TOS, it is impossible to have had 100% surface coverage of Pt by carbon. Multilayer coverage of carbon and/or carbon deposition on the support are likely to have occurred. Even though most of the carbon deposition occurred during the first 5 min on both Pt and PtFe, the carbon deposited later caused different effects on Pt and PtFe. The concentration of surface intermediates, N_{I-CO_2} , for Pt decreased rapidly, whereas that for PtFe gradually decreased. Although the amount of deposited carbon at steady state was not significantly different (125 $\mu\text{mole/g}_{\text{cat}}$ for Pt and 103 $\mu\text{mole/g}_{\text{cat}}$ for PtFe), it could be that CO adsorbed on the sites of PtFe still had more oxygen available for reaction. This idea follows from the results of Lee and Gavriilidis³² for Au/ γ -Al₂O₃ catalysts and Bulushev et al.³³ for Fe-promoted Au/C catalysts where deactivation was

decreased by either injecting excess oxygen³² or promoting the catalyst with more preferable oxygen adsorption sites³³. This idea is also consistent with the ITKA results showing that the concentration of surface intermediates on PtFe decreased at a much slower rate than that on Pt.

6. Conclusions

6.1 NCSU Conclusions

The focus of our current work has been catalyst characterization of the supports, in addition to the prior PROX reaction work, to give a holistic view of our catalyst. The characterization of the catalytic supports can be summarized as the following:

- The unwashcoated, uncatalysed blank foam and blank reactor do not uptake CO.
- Either the Fe, γ -Al₂O₃ washcoat and its surface impurities, or both, are weakly chemisorbing or physisorbing CO and causing an elongated tail during pulse chemisorption via slow bleed out to the NDIR.
- For varying Fe loading on ceramic straight-channel monoliths, lower Fe correlates to higher dispersion because of a decrease in inhibition of the Pt surface. Therefore, a lower Fe loading on the 12% ρ metal foams is postulated to explain the decrease in dispersion for the more active and selective 4% ρ metal foams in both pulse chemisorption and TPD calculations.
- The T_{des} data for CO desorption peak temperature falls into a similar range of $\sim 160^{\circ}\text{C}$ measured by Manasilp and Gulari.
- The d_{pt} results for Fe-promoted Pt/ γ -Al₂O₃ are higher than Liu et al and Sakamoto et al, indicating possible sintering of the catalysts by agglomeration.
- The TPD results are lower than the pulse chemisorption results because the latter accounts for CO adsorption on either the Fe, γ -Al₂O₃ washcoat, or both, in addition to the Pt.
- Different trials of the same catalyst under identical conditions produced inconsistent results for pulse chemisorption and TPD. For TPD, the 20 ppi, 12% ρ metal foam, first trial, revealed a bimodal peak that was irreproducible.

6.2 Clemson Conclusions

Effects of Fe promotion of Pt for the selective oxidation of CO can be summarized as the following:

- Overall reaction rate increases because of an increase in intrinsic site activity, possibly as a result of more oxygen adsorption sites and/or an increase in oxygen adsorption ability. The ITKA results support the hypothesis about an increase in oxygen adsorption ability upon Fe addition.
- With TOS, site activity of PtFe appears to asymptotically approach that of Pt indicating that the surface becomes more like Pt as deactivation occurs.

- Even though the amount of carbon deposition is similar for both catalysts, the concentration of surface intermediates on PtFe decreased at a slower rate perhaps due to Fe providing oxygen adsorption sites and increasing oxygen accessibility to adsorbed CO.
- Fe promotion does not increase the number of active sites. The maximum concentrations of active intermediates were approximately the same for both Pt and PtFe.

Although the deactivation of the Pt catalyst appears to mainly be the result of a decrease in the concentration of surface intermediates, for the PtFe catalyst, it is the result of both a decrease in the average intrinsic site activity and a decrease in the concentration of surface intermediates with the decrease in average intrinsic site activity having the biggest effect. The decrease in the concentration of carbon surface intermediates with TOS for both catalysts is probably due to carbon deposition. In case of PtFe, the intrinsic site activity decreased most likely because of a reoxidation of Fe which decreased the oxygen adsorption ability. The intrinsic site activity of PtFe approached that of Pt with TOS as the Fe promotion effect was diminished.

7. Recommendations

7.1 NCSU Recommendations

- a) Determine the cause of the elongated tail in pulse chemisorption. Either the γ -Al₂O₃ washcoat, Fe, or both, is the source of the CO bleeding seen in the pulses. Retest the catalysts, with and without the presence of Fe, the next day, after saturation by chemisorption the day prior, to see if there is any more uptake of CO. If there is no uptake of CO from the catalyst with no Fe, but uptake of CO from the catalyst with Fe, then it is the Fe that is the cause of the elongated tail. If uptake of CO occurs on both the Fe and non-Fe catalysts, then it is the support causing the elongated tail.
- b) Determine the cause for increased error at higher pure N₂ flow rates. Either the NDIR is flow rate dependent, or the mass flow controller is not outputting the correct N₂ flow rate on the control and readout equipment. Use the span gas, or the wet test meter and/or soap bubble flow meter, respectively, to test the equipment.
- c) Finish the pulse chemisorption and TPD tests. This gives a robust data set that will elucidate the differences in activity and selectivity seen on the various supports.
- d) Conduct other catalyst characterization techniques that are destructive to our catalyst: scanning electron microscopy (SEM), transmission electron microscopy (TEM), x-ray photoelectron spectroscopy (XPS), inductively coupled plasma (ICP), extended x-ray absorption fine structure (EXAFS), and other potential techniques.
- e) Develop a reproducible catalyst preparation technique. The Pt/Fe system investigated by NCSU appears to have promise, but there is a lot of variance in the activity and selectivity of the metal foam supports. Re-evaluate other support structures once a reproducible catalyst preparation technique is established.

7.2 Clemson Recommendations

- f) Determine a relationship between temperature and selectivity to help explain the differences in CO₂ selectivity for the PtFe metal foams.
- g) Determine how the impurity affects CO₂ selectivity using energy dispersive x-ray spectroscopy (EDX) results.
- h) Obtain more BET and chemisorption results.
- i) Measure how the variation in activity and selectivity for different metal foam catalyst samples.
- j) Complete ITKA comparison of reaction on the metal foam catalysts to those on the powdered catalysts.

8. References

1. Rohland, B. and V. Plzak, *The PEMFC-integrated CO oxidation - a novel method of simplifying the fuel cell plant*. Journal of Power Sources, 1999. **84**(2): p. 183-186.
2. Gotz, M. and H. Wendt, *Binary and ternary anode catalyst formulations including the elements W, Sn and Mo for PEMFCs operated on methanol or reformat gas*. Electrochimica Acta, 1998. **43**(24): p. 3637-3644.
3. Avgouropoulos, G., et al., *A comparative study of Pt/gamma-Al₂O₃, Au/alpha-Fe₂O₃ and CuO-CeO₂ catalysts for the selective oxidation of carbon monoxide in excess hydrogen*. Catalysis Today, 2002. **75**(1-4): p. 157-167.
4. Manasilp, A. and E. Gulari, *Selective CO oxidation over Pt/alumina catalysts for fuel cell applications*. Applied Catalysis B-Environmental, 2002. **37**(1): p. 17-25.
5. Sirijaruphan, A., J.G. Goodwin, and R.W. Rice, *Investigation of the Initial Rapid Deactivation of Platinum Catalysts during the Selective Oxidation of Carbon Monoxide*. Journal of Catalysis, in press.
6. Korotkikh, O. and R. Farrauto, *Selective catalytic oxidation of CO in H₂: Fuel cell applications*. Catalysis Today, 2000. **62**(2-3): p. 249-254.
7. Liu, X.S., O. Korotkikh, and R. Farrauto, *Selective catalytic oxidation of CO in H₂: structural study of Fe oxide-promoted Pt/alumina catalyst*. Applied Catalysis a-General, 2002. **226**(1-2): p. 293-303.
8. Son, I.H. and A.M. Lane, *Promotion of Pt/gamma-Al₂O₃ by Ce for preferential oxidation of CO in H₂*. Catalysis Letters, 2001. **76**(3-4): p. 151-154.
9. Kahlich, M.J., H.A. Gasteiger, and R.J. Behm, *Kinetics of the selective CO oxidation in H₂-rich gas on Pt/Al₂O₃*. Journal of Catalysis, 1997. **171**(1): p. 93-105.
10. Shannon, S.L. and J.G. Goodwin, *Characterization of Catalytic Surfaces by Isotopic-Transient Kinetics During Steady-State Reaction*. Chemical Reviews, 1995. **95**(3): p. 677-695.
11. Chen, B. and J.G. Goodwin, *Isotopic Transient Kinetic-Analysis of Ethane Hydrogenolysis on Ru/SiO₂*. Journal of Catalysis, 1995. **154**(1): p. 1-10.
12. Hoost, T.E. and J.G. Goodwin, *Nonparametric Determination of Reactivity Distributions from Isotopic Transient Kinetic Data*. Journal of Catalysis, 1992. **134**(2): p. 678-690.

13. White, M.G., *Heterogeneous Catalysis*. Prentice Hall International Series in the Physical and Chemical Engineering Series, ed. N.R. Amundson. 1990, Englewood Cliffs, NJ: Prentice Hall, Inc. 251.
14. Chafik, T., et al., *Heat of adsorption of carbon monoxide on a Pt/Rh/CeO₂/Al₂O₃ three-way catalyst using in-situ infrared spectroscopy at high temperatures*. Journal of Catalysis, 1998. **179**(2): p. 503-514.
15. Bourane, A., O. Dulaurent, and D. Bianchi, *Comparison of the coverage of the linear CO species on Pt/Al₂O₃ measured under adsorption equilibrium conditions by using FTIR and mass spectroscopy*. Journal of Catalysis, 2000. **195**(2): p. 406-411.
16. Sorescu, D.C., et al., *First-principles calculations of the adsorption, diffusion, and dissociation of a CO molecule on the Fe(100) surface*. Physical Review B, 2002. **66**(3).
17. Cameron, S.D. and D.J. Dwyer, *A Study of Pi-Bonded Co on Fe(100)*. Langmuir, 1988. **4**(2): p. 282-288.
18. Farrauto, R.J. and C.H. Bartholomew, *Fundamentals of Industrial Catalytic Processes*. First Edition ed. 1997, London, UK: Blackie Academic & Professional (an imprint of Chapman & Hall). 754.
19. Wachs, I.E., *Characterization of Catalytic Materials*. Materials Characterization Series (Surfaces, Interfaces, Thin Films), ed. J. C. Richard Brundle and Charles A. Evans. 1992, Stoneham, MA and Greenwich, CT: Butterworth-Heinemann and Manning Publications Co. 202.
20. *Zeton Altamira Notes*. Surface Area Measurement from Temperature-Programmed Desorption Data. Vol. 1.2, Pittsburgh, PA: Zeton Altamira.
21. Sakamoto, Y., et al., *Effect of the addition of Fe on catalytic activities of Pt/Fe/gamma-Al₂O₃ catalyst*. Applied Catalysis B-Environmental, 1999. **23**(2-3): p. 159-167.
22. Blanchard, A.A., *The Volatile Metal Carbonyls*. Chemical Review, 1937. **21**(1): p. 3-38.
23. *Zeton Altamira Notes*. Temperature-Programmed Desorption of Adsorbed Species from Catalyst Surfaces. Vol. 1.3, Pittsburgh, PA: Zeton Altamira.
24. Anderson, J.R., *Structure of Metallic Catalysts*. 1975, London, UK: Academic Press Inc. 469 pages.
25. Jia, J.F., et al., *A study on reduction behaviors of the supported platinum-iron catalysts*. Journal of Molecular Catalysis a-Chemical, 1999. **138**(2-3): p. 177-184.

26. Raab, C., et al., *Preparation and Characterization of Silica-Supported Ni/Pt Catalysts*. Journal of Catalysis, 1990. **122**(2): p. 406-414.
27. Shen, S.C. and S. Kawi, *Mechanism of selective catalytic reduction of NO in the presence of excess O₂ over Pt/Si-MCM-41 catalyst*. Journal of Catalysis, 2003. **213**(2): p. 241-250.
28. Paulis, M., H. Peyrard, and M. Montes, *Influence of chlorine on the activity and stability of Pt/Al₂O₃ catalysts in the complete oxidation of toluene*. Journal of Catalysis, 2001. **199**(1): p. 30-40.
29. Miller, J.T., et al., *Hydrogen Temperature-Programmed Desorption (H₂ Tpd) of Supported Platinum Catalysts*. Journal of Catalysis, 1993. **143**(2): p. 395-408.
30. Okamoto, H., *Desk Handbook: Phase Diagrams for Binary Alloys*. 2000, Materials Park, OH: ASM International. 828 pages.
31. Nibbelke, R.H., et al., *Kinetic study of the CO oxidation over Pt/gamma-Al₂O₃ and Pt/Rh/CeO₂/gamma-Al₂O₃ in the presence of H₂O and CO₂*. Journal of Catalysis, 1997. **171**(2): p. 358-373.
32. Lee, S.J. and A. Gavriilidis, *Supported Au catalysts for low-temperature CO oxidation prepared by impregnation (vol 206, pg 305, 2002)*. Journal of Catalysis, 2002. **211**(1): p. 283-283.
33. Bulushev, D.A., et al., *Structured Au/FeOX/C catalysts for low-temperature CO oxidation*. Journal of Catalysis, 2002. **210**(1): p. 149-159.

9. Bibliography

Anderson, J.R., *Structure of Metallic Catalysts*. 1975, London,UK: Academic Press Inc. 469 pages.

Farrauto, R.J. and C.H. Bartholomew, *Fundamentals of Industrial Catalytic Processes*. First Edition ed. 1997, London, UK: Blackie Academic & Professional (an imprint of Chapman & Hall). 754.

Okamoto, H., *Desk Handbook: Phase Diagrams for Binary Alloys*. 2000, Materials Park, OH: ASM International. 828 pages.

Wachs, I.E., *Characterization of Catalytic Materials*. Materials Characterization Series (Surfaces, Interfaces, Thin Films), ed. J. C. Richard Brundle and Charles A. Evans. 1992, Stoneham, MA and Greenwich, CT: Butterworth-Heinemann and Manning Publications Co. 202.

White, M.G., *Heterogeneous Catalysis*. Prentice Hall International Series in the Physical and Chemical Engineering Series, ed. N.R. Amundson. 1990, Englewood Cliffs, NJ: Prentice Hall, Inc. 251.

Zeton Altamira Notes. Surface Area Measurement from Temperature-Programmed Desorption Data. Vol. 1.2, Pittsburgh, PA: Zeton Altamira.

Zeton Altamira Notes. Temperature-Programmed Desorption of Adsorbed Species from Catalyst Surfaces. Vol. 1.3, Pittsburgh, PA: Zeton Altamira.

10. List of Acronyms and Abbreviations

<u>Abbreviation</u>	<u>Definition</u>
40/4	40 ppi, 4% ρ metal foam
20/4	20 ppi, 4% ρ metal foam
20/12	20 ppi, 12% ρ metal foam
40/12	40 ppi, 12% ρ metal foam
ΔH_{rxn}	Heat of reaction
ΔT_{ad}	Adiabatic temperature rise
τ	Residence time
BET	Brunauer-Emmett-Teller
C_p	Heat capacity
cpsi	Cells per square inch
d_{Pt}	Average Pt crystallite size
DRIFTS	Diffuse reflectance infrared fourier transform spectroscopy
EDX	Energy dispersive x-ray spectroscopy
FID	Flame ionization detector
FSB	Fluidized sand bath
GHSV	Gas hourly space velocity
HRTEM	High resolution transmission electron microscopy
I.D.	Inner diameter
ITKA	Isotopic transient kinetic analysis
MFC	Mass flow controller
NDIR	Nondispersive infrared
$n_{\text{CO,loop}}$	Moles of CO calculated in the sample loop
$n_{\text{CO,NDIR pulse}}$	Moles of CO calculated from the NDIR detector and N_2 flow rate
ppi	Pores per inch
PROX	Preferential oxidation
r-WGS	Reverse water-gas-shift
S_{CO}	CO selectivity
S_g	Maximum surface area possible per gram metal basis ($\text{cm}^2/\text{g metal}$)

<u>Abbreviation</u>	<u>Definition</u>
sccm	Standard cubic centimeter per minute (273 K, 101 kPa, cm ³ /min)
T _{des}	Desorption temperature peak for TPD
T _{in}	Reactor inlet temperature
TEM	Transmission electron microscopy
TCD	Thermal conductivity detector
TOF	Turnover frequency
TOS	Time-on-stream
TPD	Temperature-programmed desorption
TPR	Temperature programmed reduction
UHP	Ultra-high pure
VV	Variac voltmeter transformer
X _{CO}	CO conversion
X _{O₂}	O ₂ conversion
XRD	X-ray diffraction

APPENDICES

APPENDIX A METAL FOAM PICTURES



Figure A.1: Different shapes of metal foams.

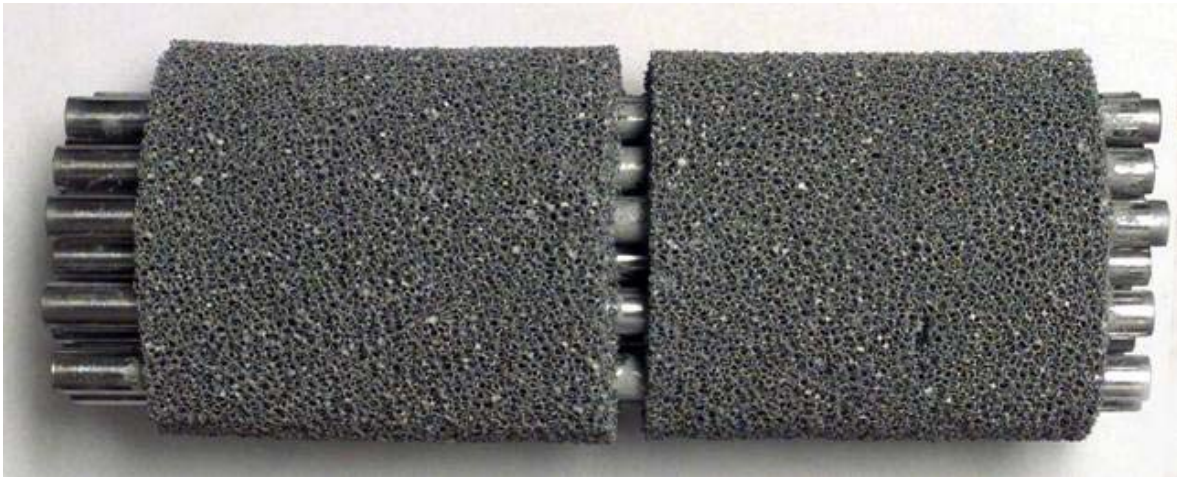


Figure A.2: Metal foams inserted with metal tubes.

Figure B.1: Reaction reactor design schematic.

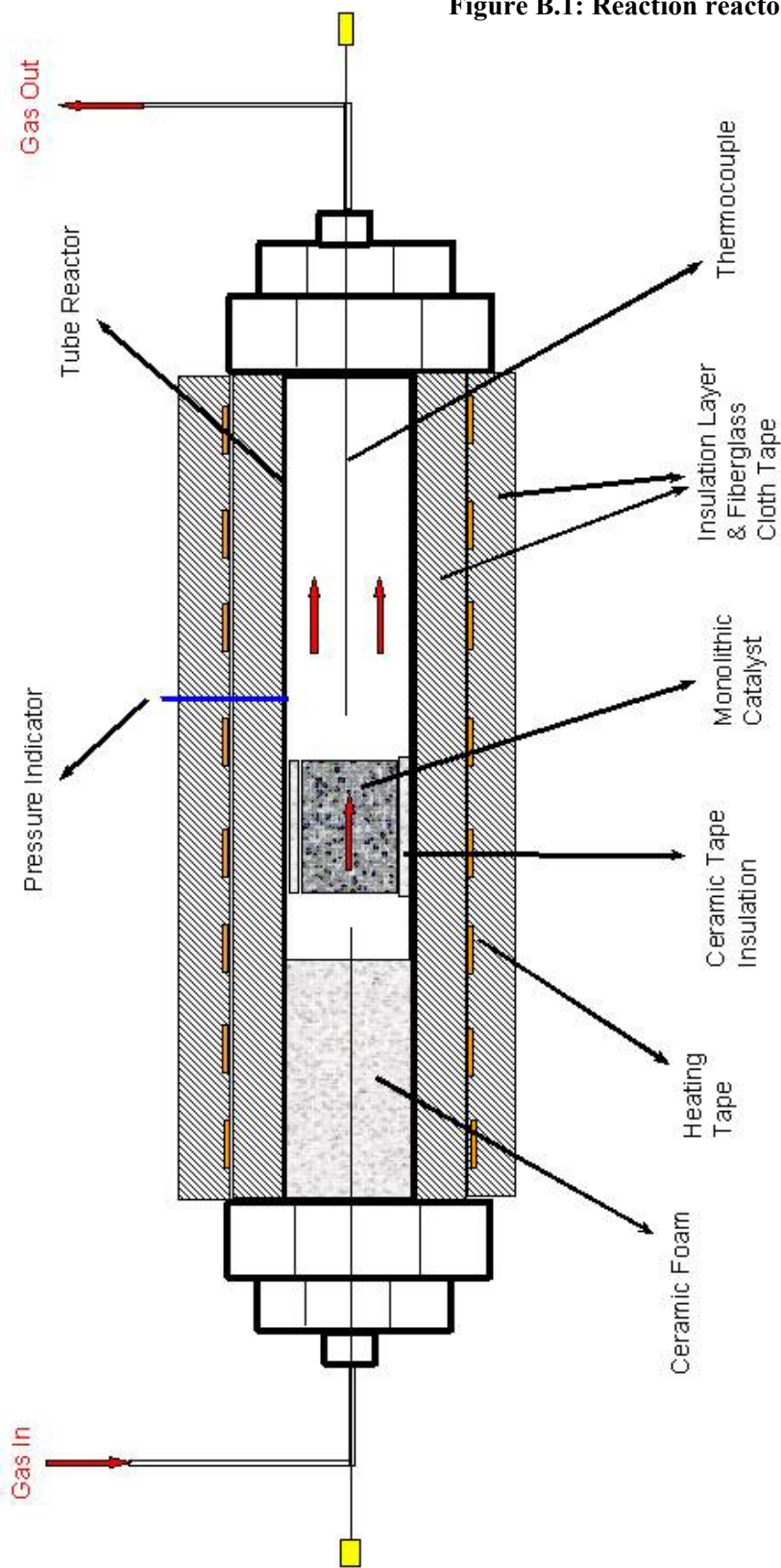


Figure B.2: Reaction reactor design dimensions.

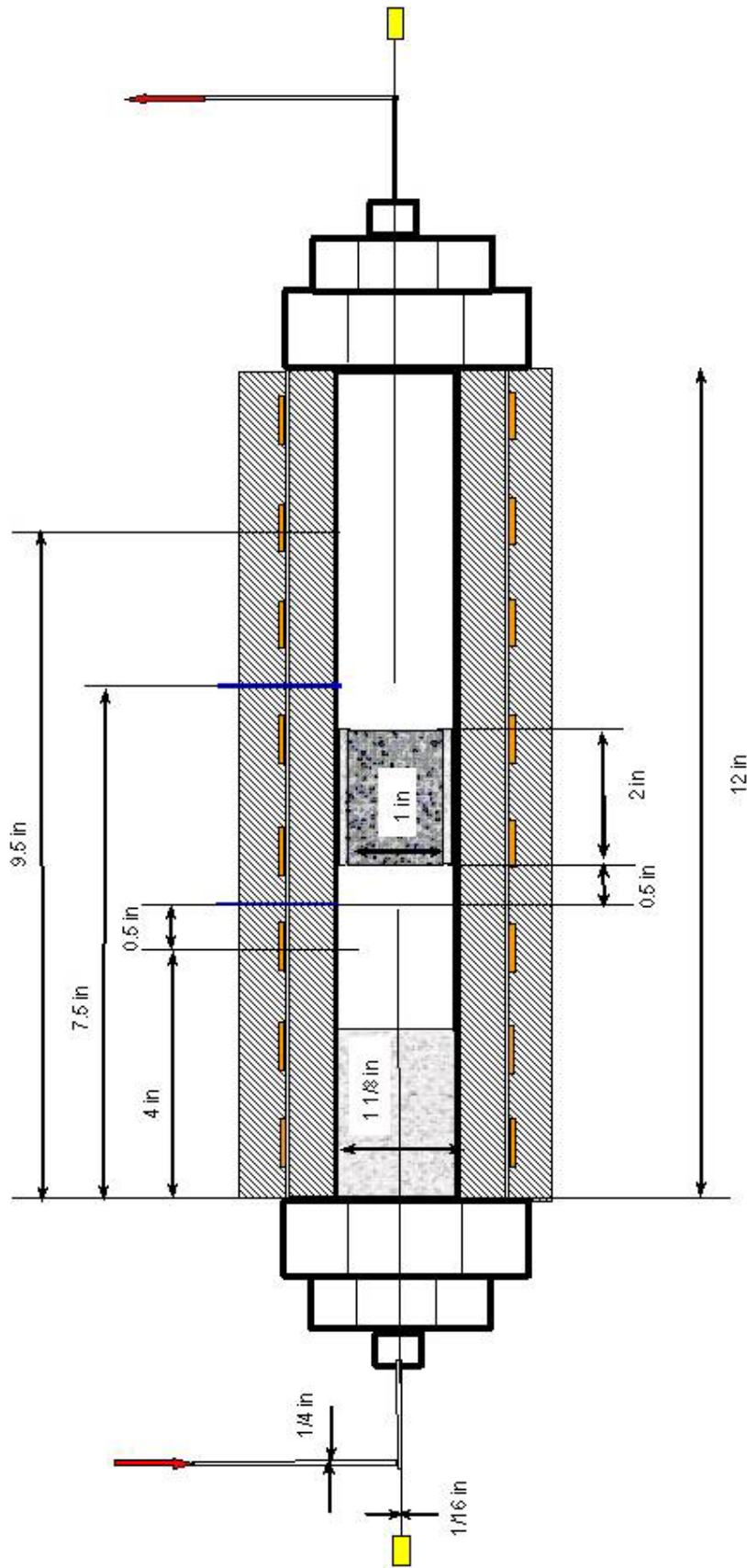


Figure B.3: Characterization reactor design schematic.

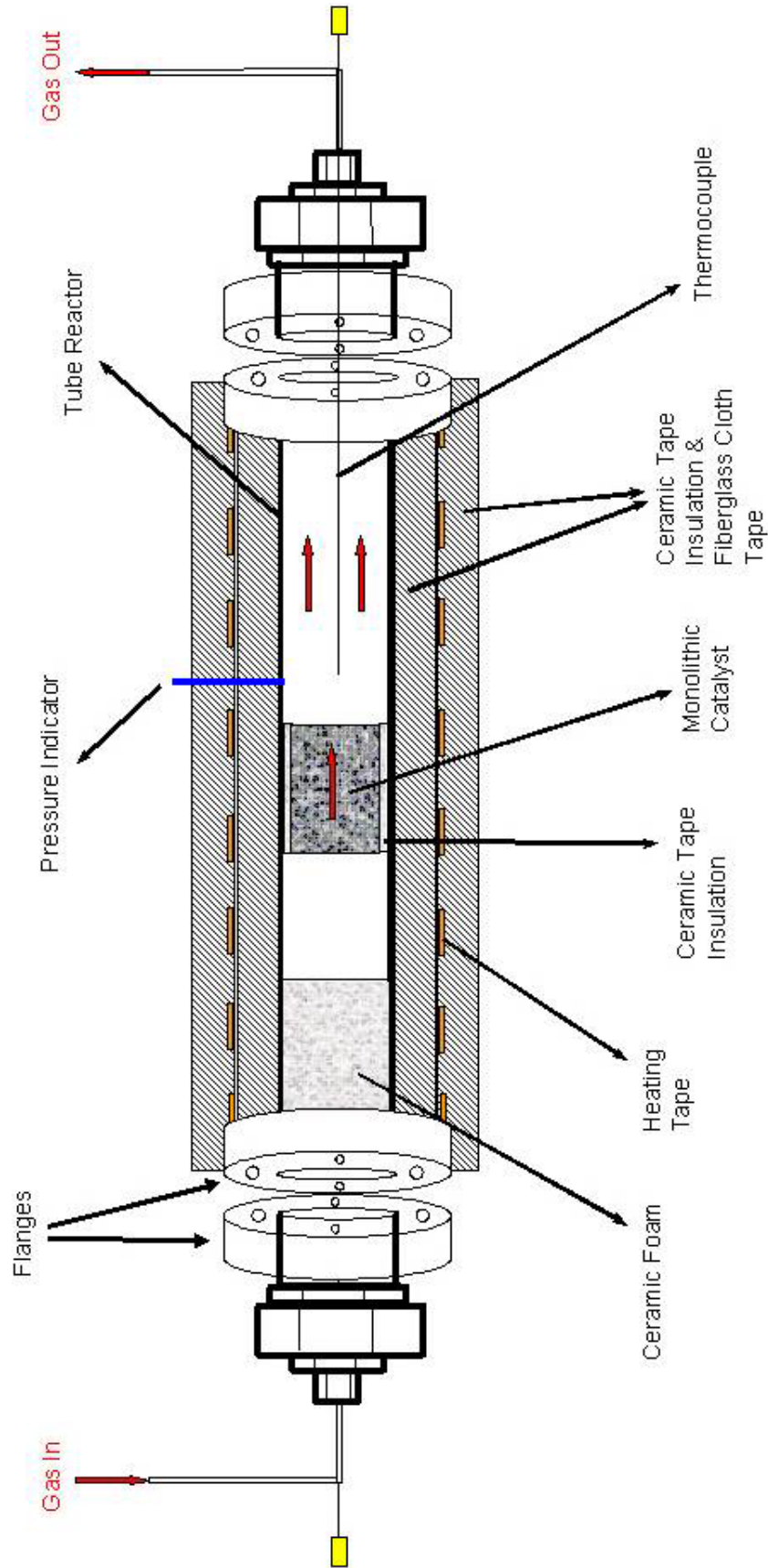


Figure B.4: Characterization reactor design dimensions.

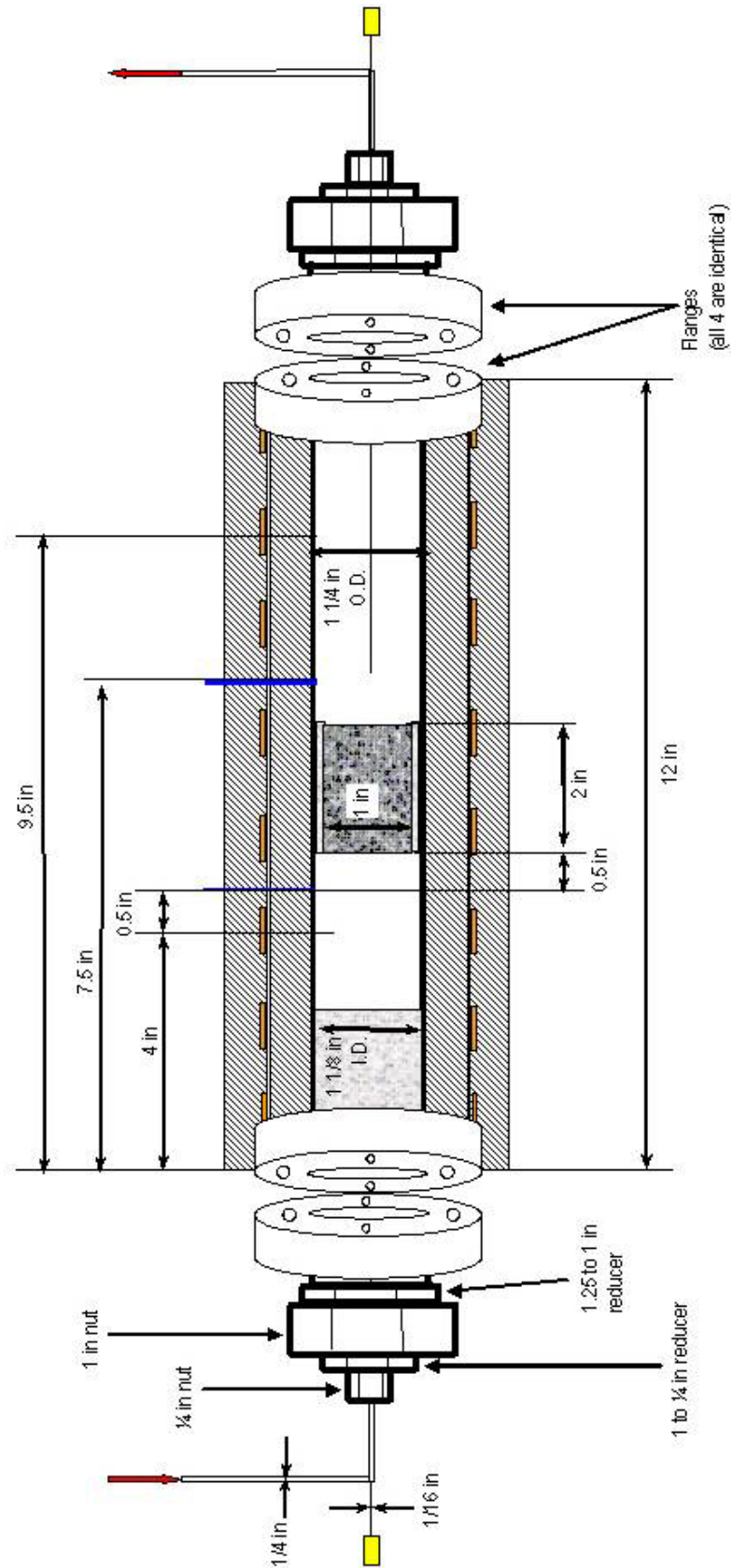


Figure B.5: Characterization reactor flange and gasket dimensions

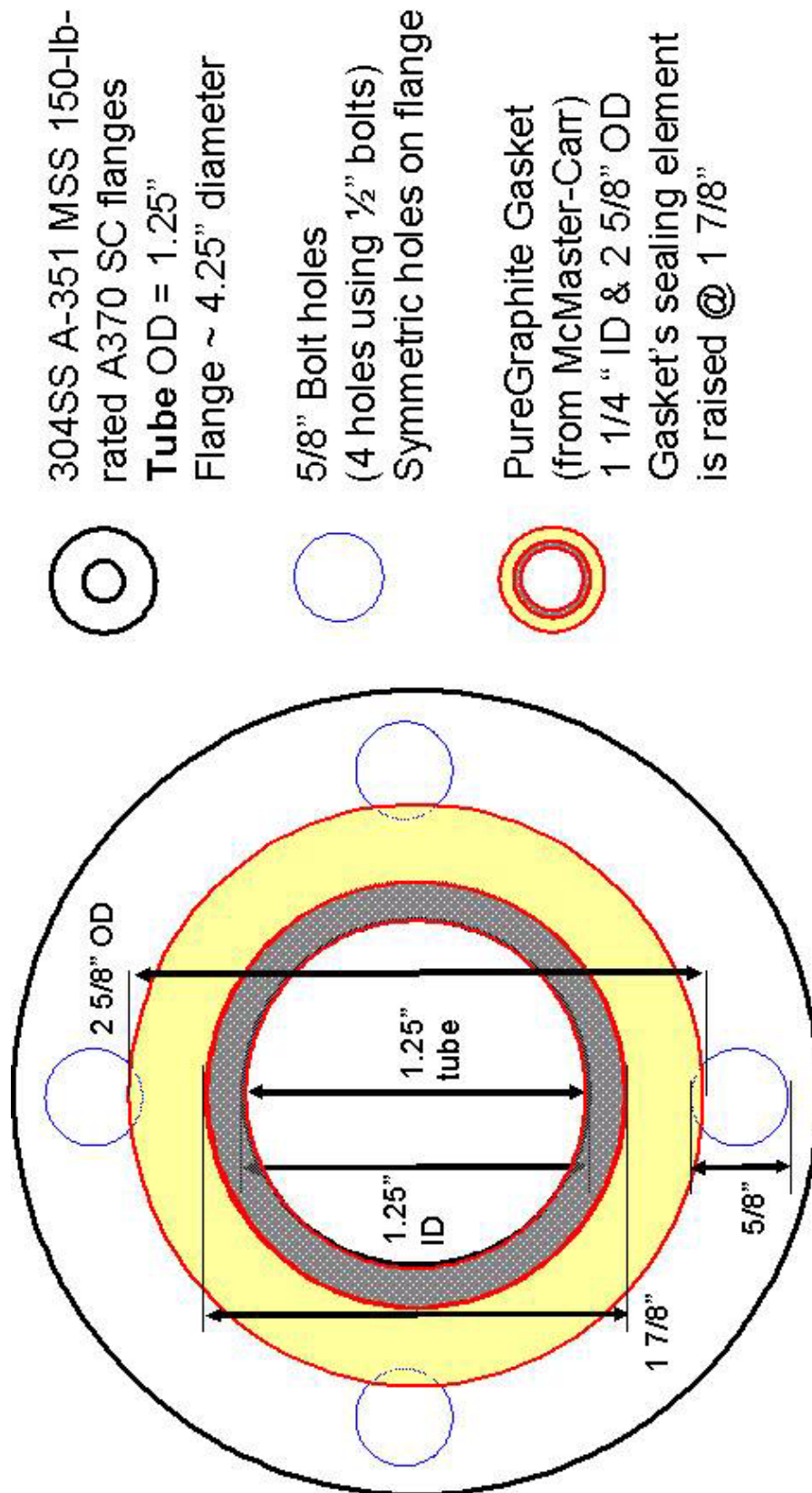
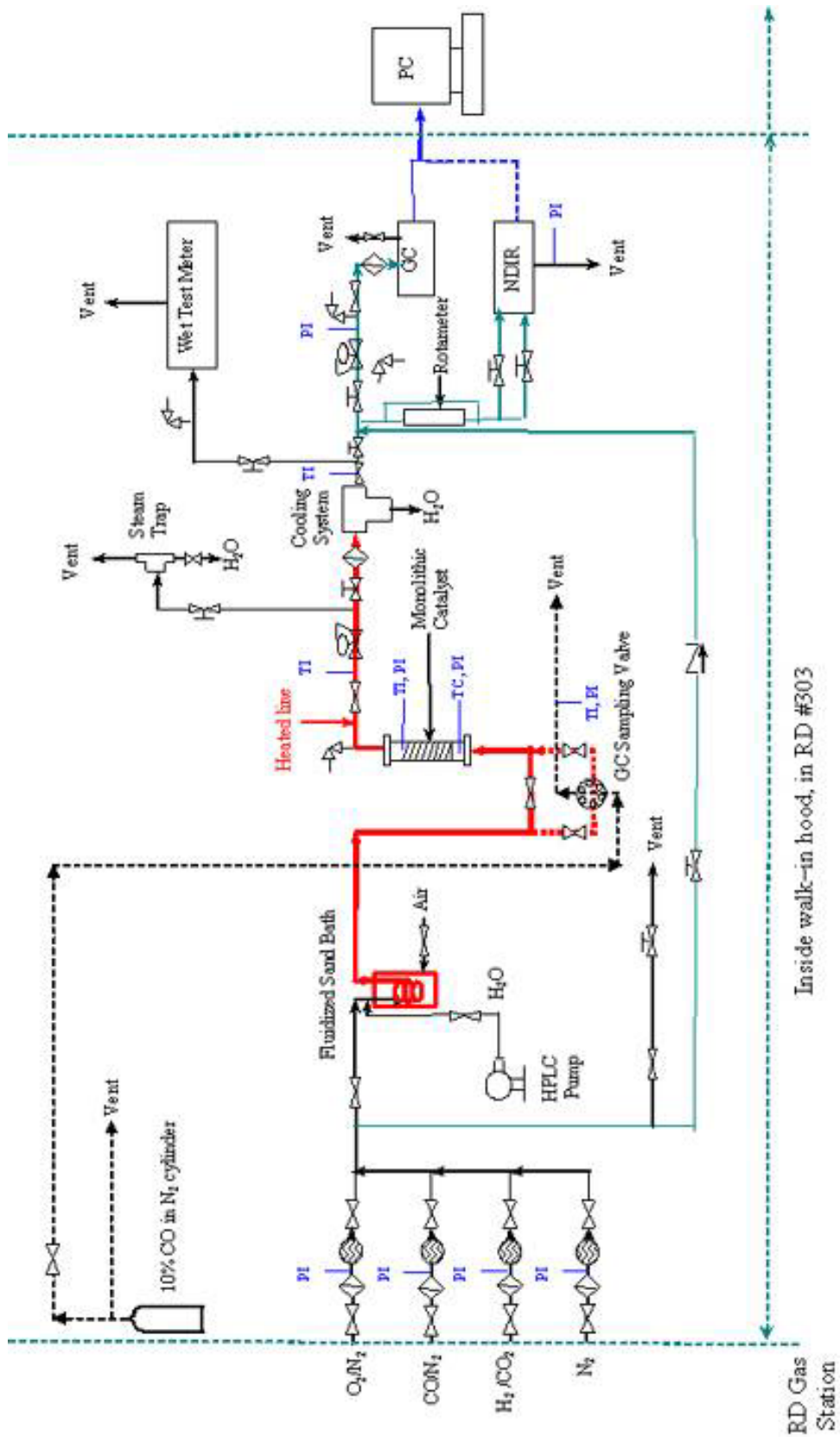









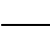



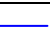


Figure B.6: Process Flow Diagram



Process Flow Diagram Notation

 : Regular valve;	 : Back pressure regulator;
 : Regular valve;	 : Front pressure regulator;
 : Mass flow rate controller;	 : Needle Valve;
 : Pressure relieve valve;	 : Check Valve;
 : Filter (7 micro meters);	 : Main flow line (black);
 : GC Sampling Valve	 : Heated line (red);
TI : Temperature indicator;	 : Gas sampling line (green);
TC : Temperature controller;	 : Cable line (blue);
PI : Pressure indicator;	

APPENDIX C CLEMSON FIGURES

Table C.1: Characterization results for the Pt and PtFe catalysts.

Catalyst	BET surface area	H _{irr}	CO _{irr}	% Dispersion
	m ² /g _{cat}	μmole H atoms/g _{cat}	μmole CO/g _{cat}	
5% Pt/Al	230	116	127	45.4 ^a
5%Pt/0.5%Fe/Al	233	83	77	32.3 ^a (24.2 ^b)

^a Calculated from the amount of irreversibly adsorbed hydrogen assuming H_{irr}/Pt_s=1.

^b Calculated consider both Pt and Fe and assuming H_{irr}/Pt_s=1 and H_{irr}/Fe_s=1.

Table C.2: Activity and selectivity of Pt and PtFe at different feed compositions.

Catalyst	P _O kPa	P _{CO} kPa	Reaction Rate(μmole/g _{cat} /s)		% CO ₂ Selectivity	
			initial	steady state	initial	steady state
			Pt	0.9	1.8	6.6
	1.8	1.8	8.3	0.9	91	27
	3.6	1.8	9.3	1.3	61	17
	0.9	0.9	5.1	0.6	39	20
	3.6	3.6	8.6	2.0	42	25
PtFe	0.9	1.8	25.7	4.2	88	64
	1.8	1.8	48.2	4.3	73	50
	3.6	1.8	50.2	4.3	25	40
	0.9	0.9	14.6	4.1	50	56
	3.6	3.6	53.6	5.6	59	60

Figure Captions

- Figure C.1:** Temperature programmed reduction profiles of Pt and PtFe compared to an Fe catalyst.
- Figure C.2:** Temperature programmed desorption of gas mixture (1%CO, 45% H₂ in He) on Pt, PtFe and Fe catalyst.
- Figure C.3:** a) CO oxidation rate b) H₂ oxidation rate and c) CO₂ selectivity of the Pt and PtFe catalysts.
- Figure C.4:** Effect of pre-exposing to a stream of O₂/He or CO/He on a) Pt and b) PtFe catalysts.
- Figure C.5:** Typical normalized transient response.
- Figure C.6:** Time-on-stream behavior of a) the pseudo-first-order intrinsic rate constant and b) concentration of surface CO₂ intermediates of Pt and PtFe for P_{O₂} =1.8 kPa.
- Figure C.7:** Amount of carbon deposited on PtFe with time-on-stream.
- Figure C.8:** a) Rate constant distribution b) shift of total CO₂ intermediates of the PtFe catalyst at different time-on-streams.
- Figure C.9:** Rate constant distribution of the Pt and PtFe catalysts at a) 5 min TOS and b) steady state.

Figure C.1

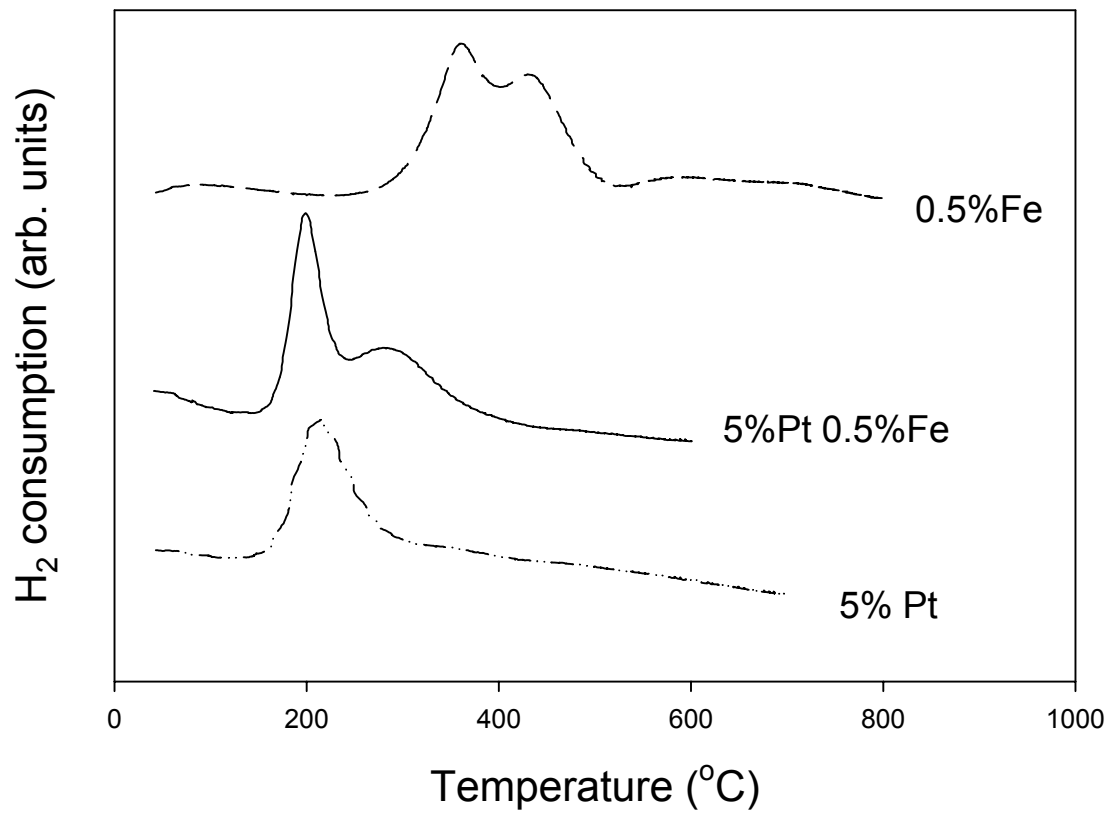


Figure C.2

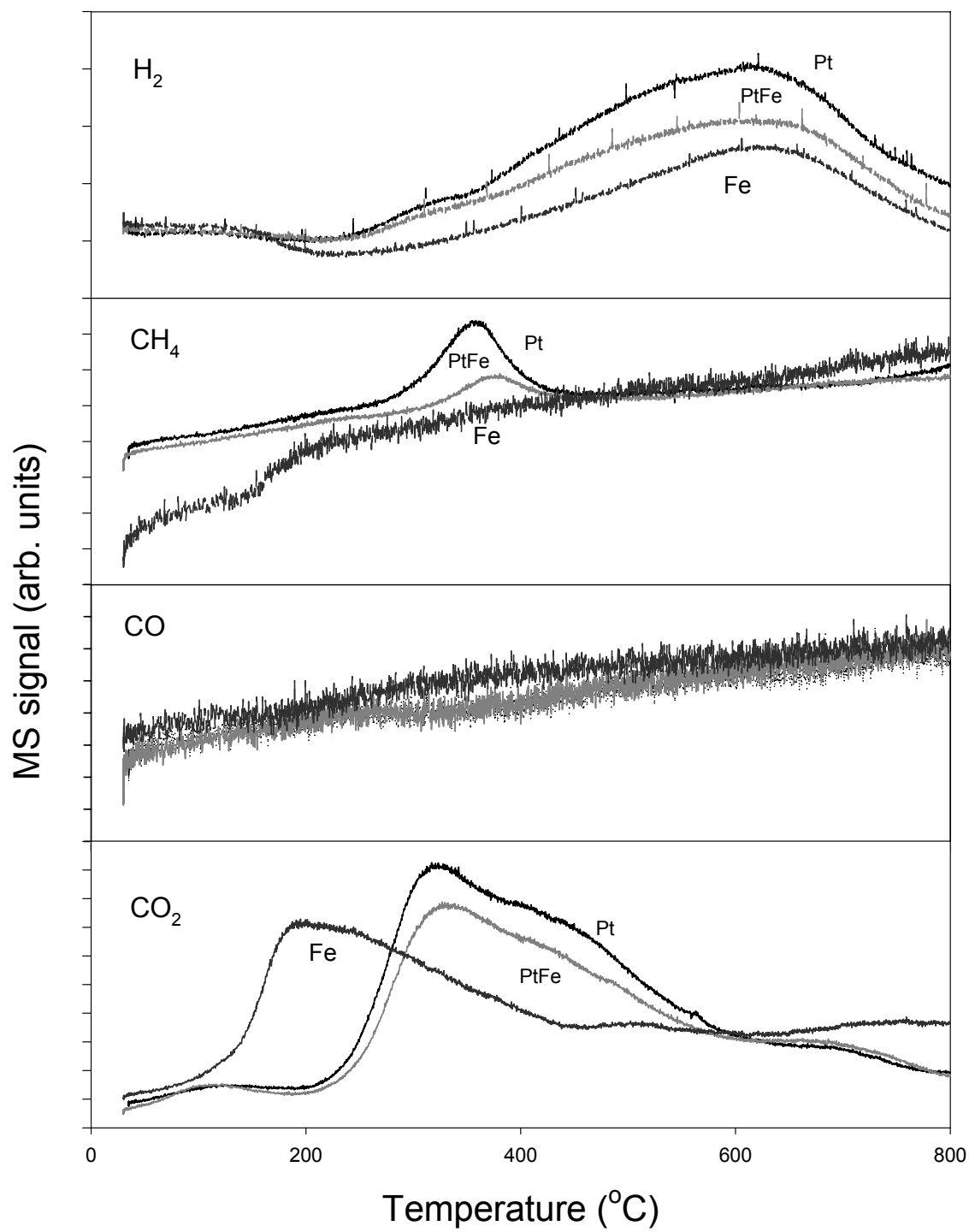


Figure C.3

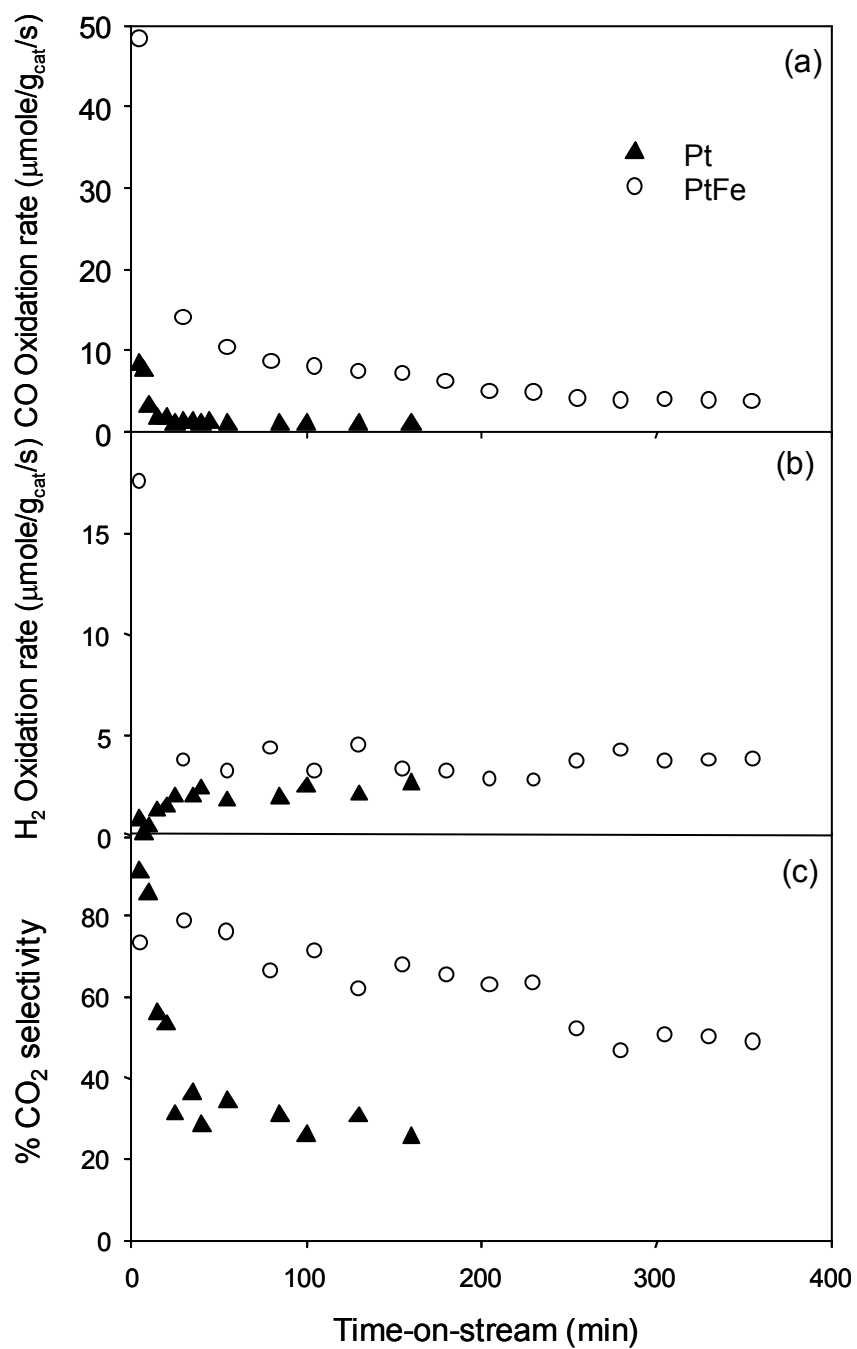


Figure C.4

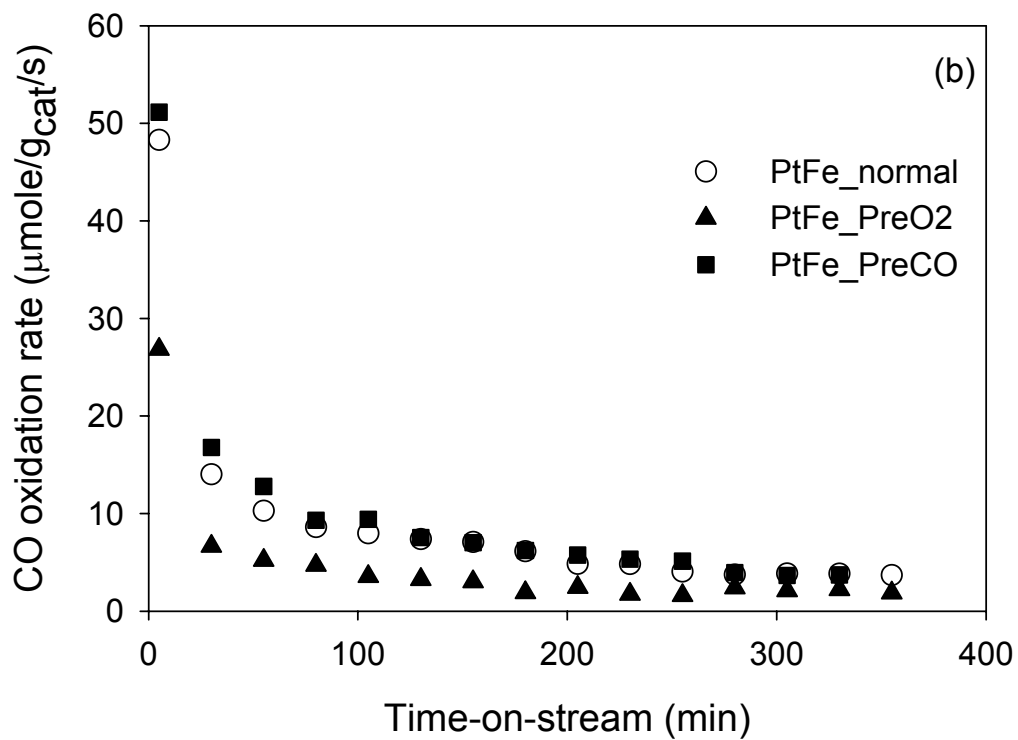
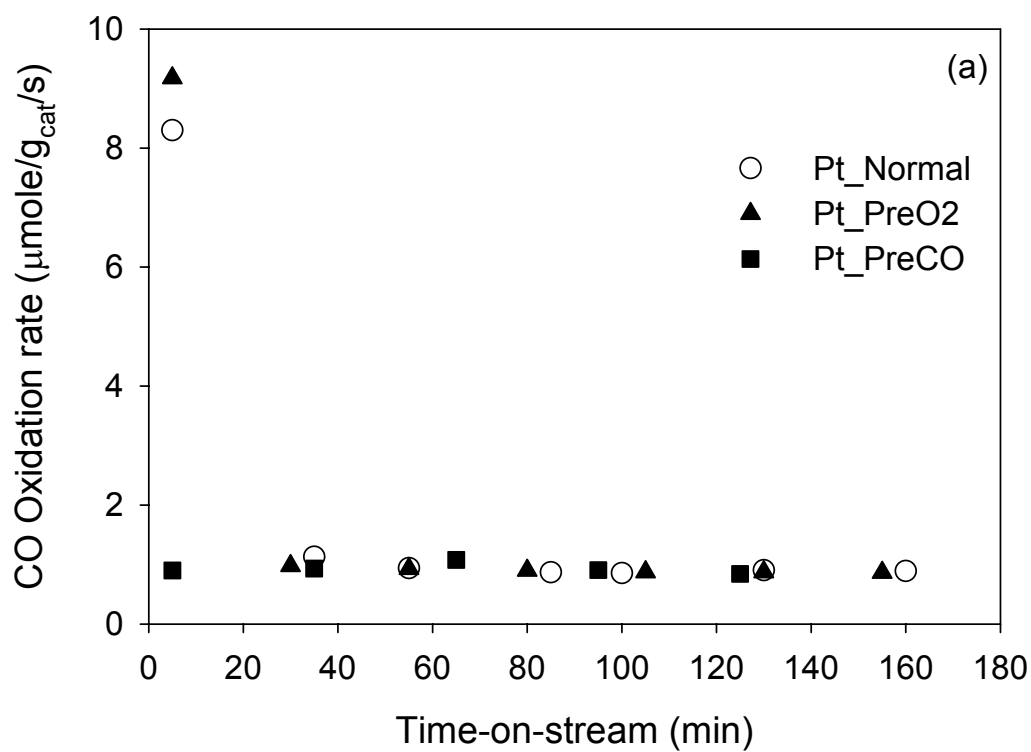


Figure C.5

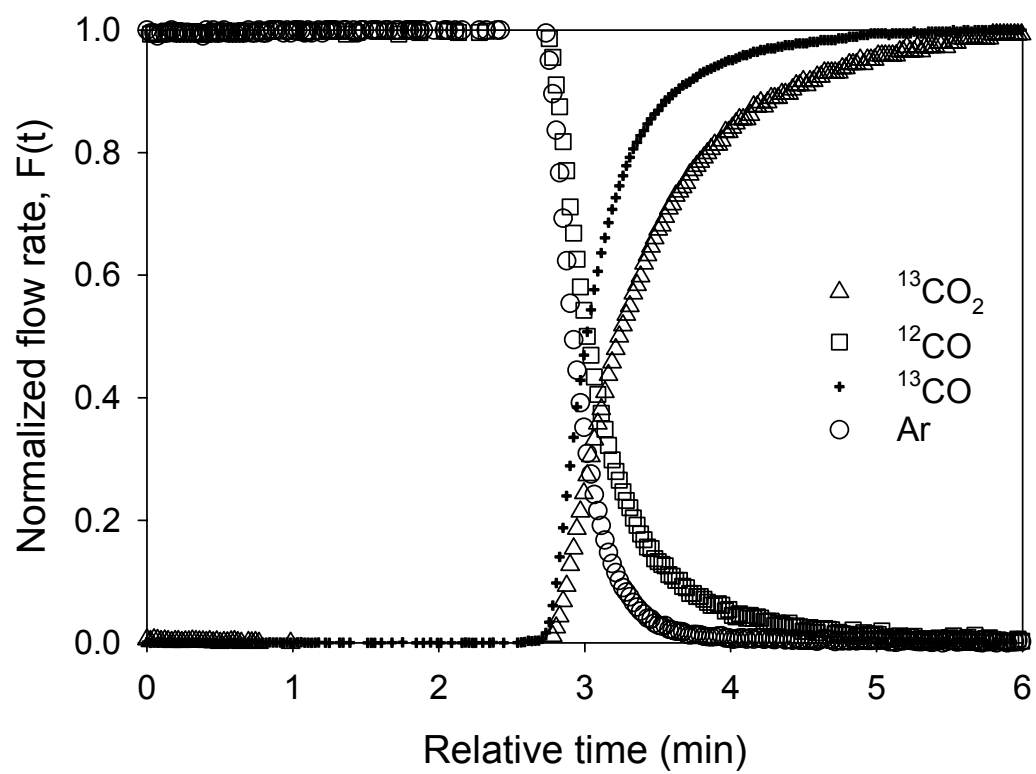


Figure C.6

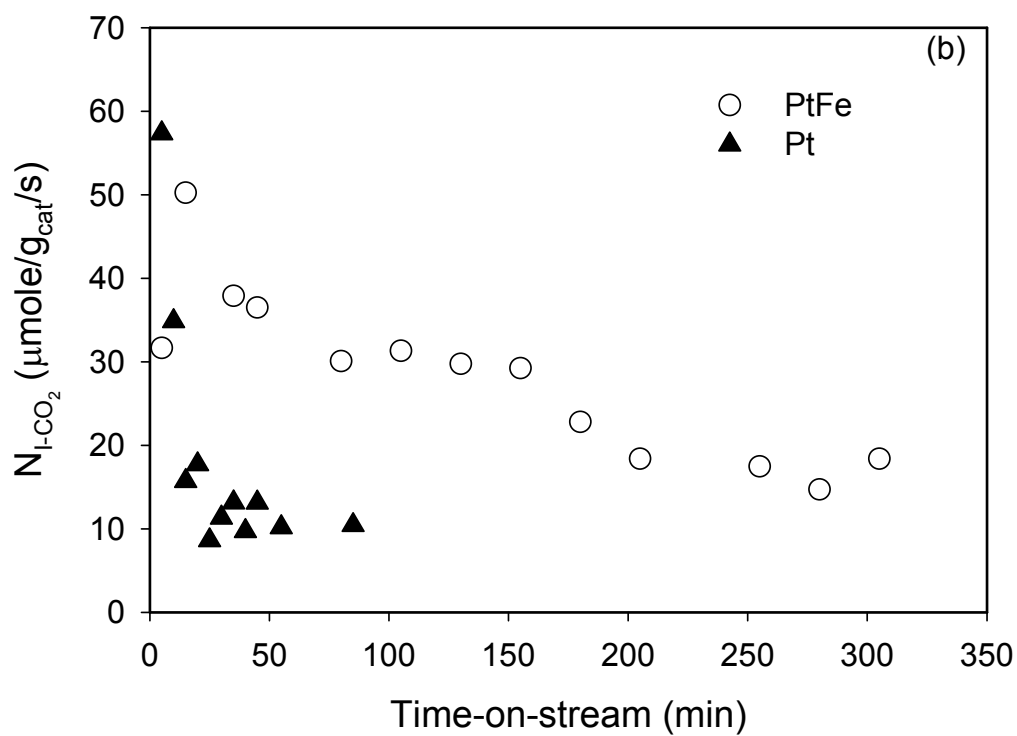
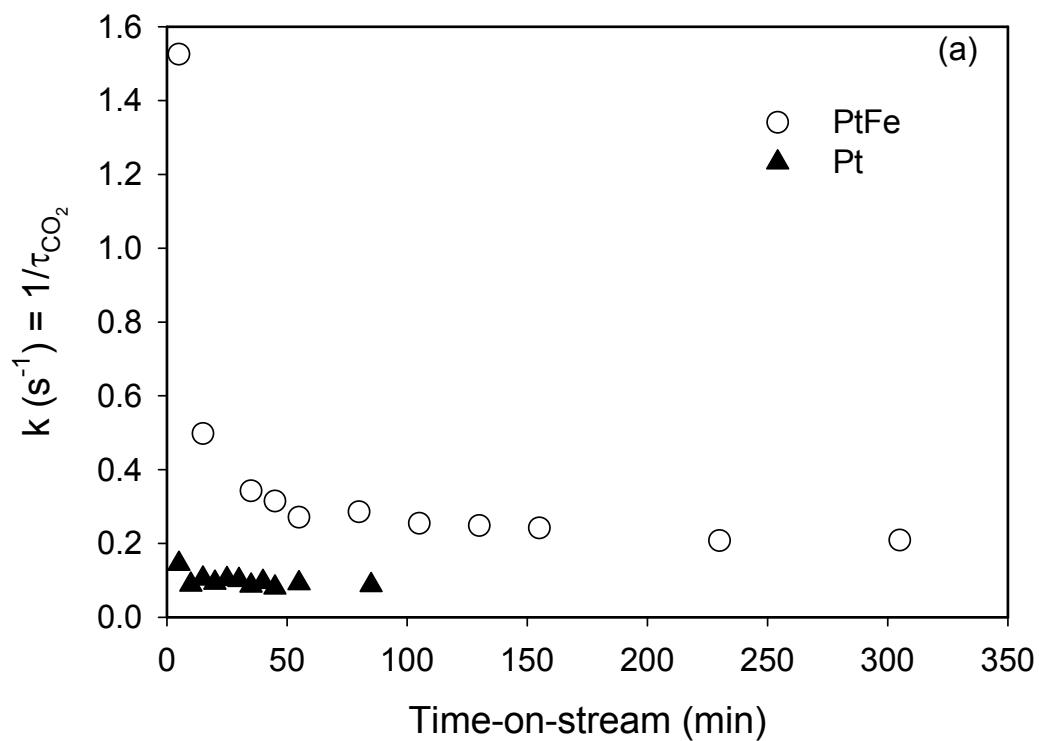


Figure C.7

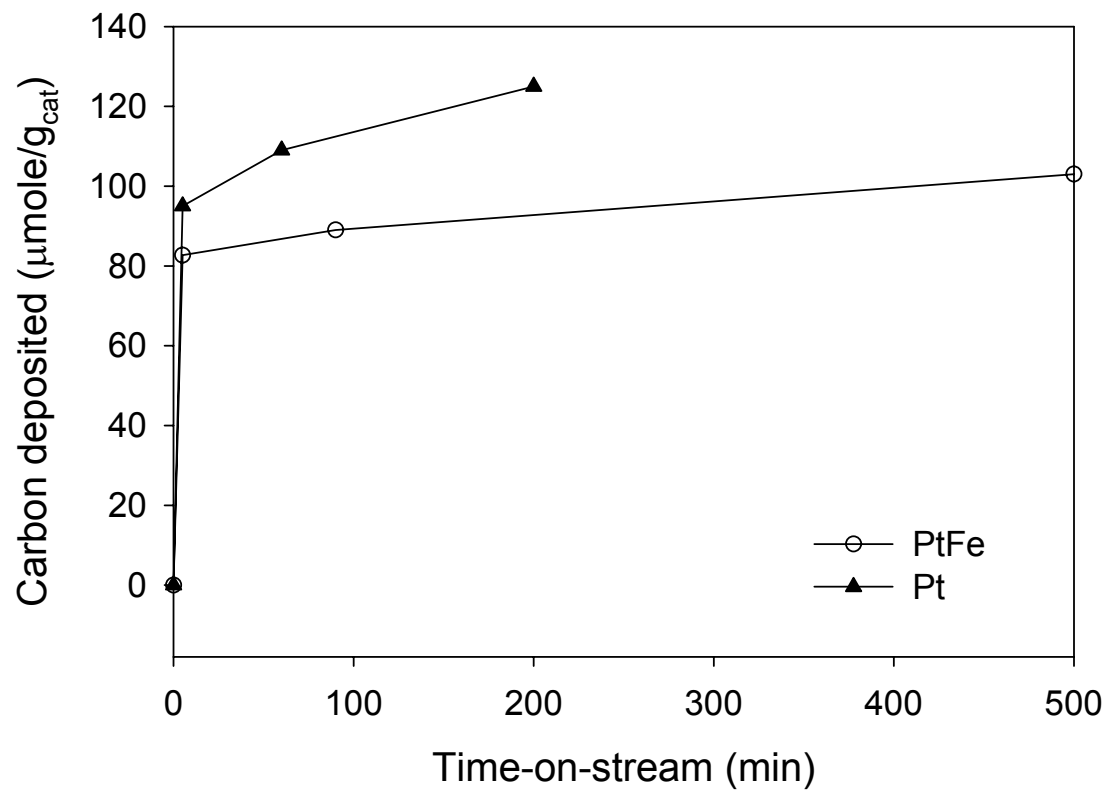


Figure C.8

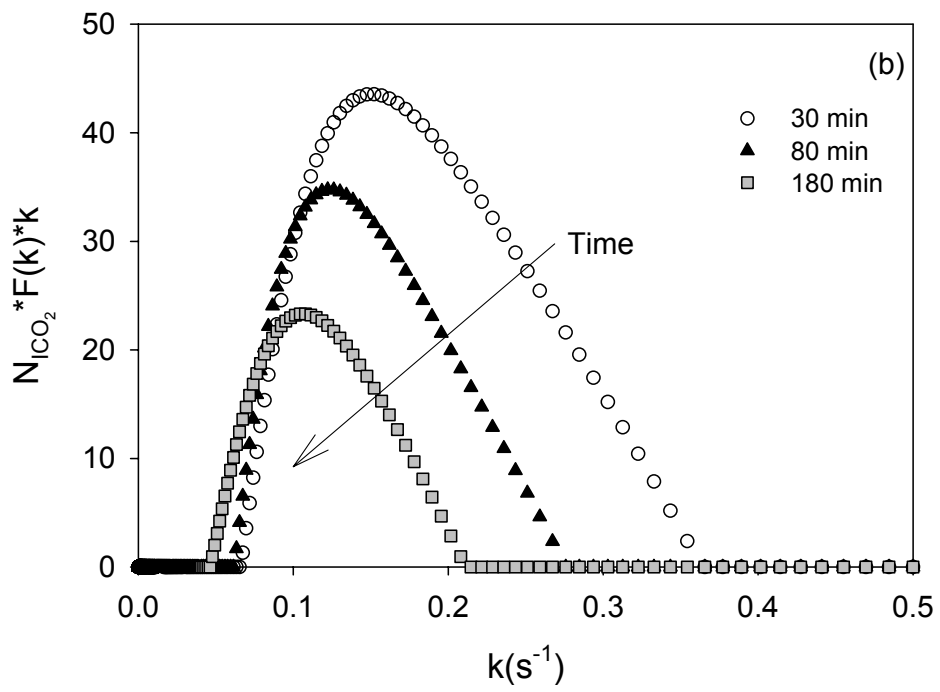
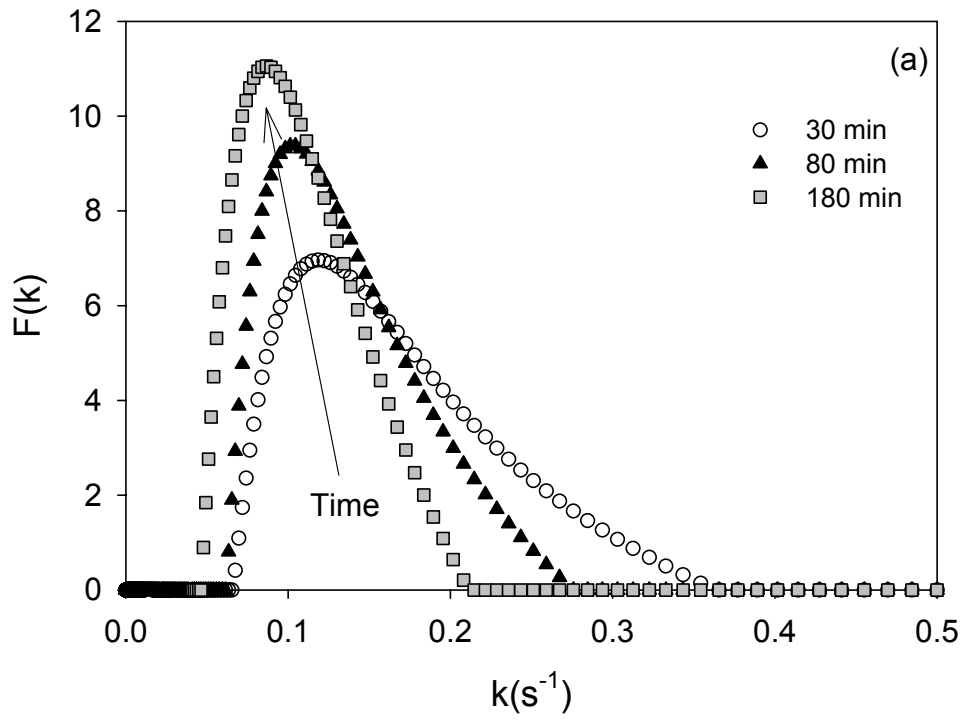
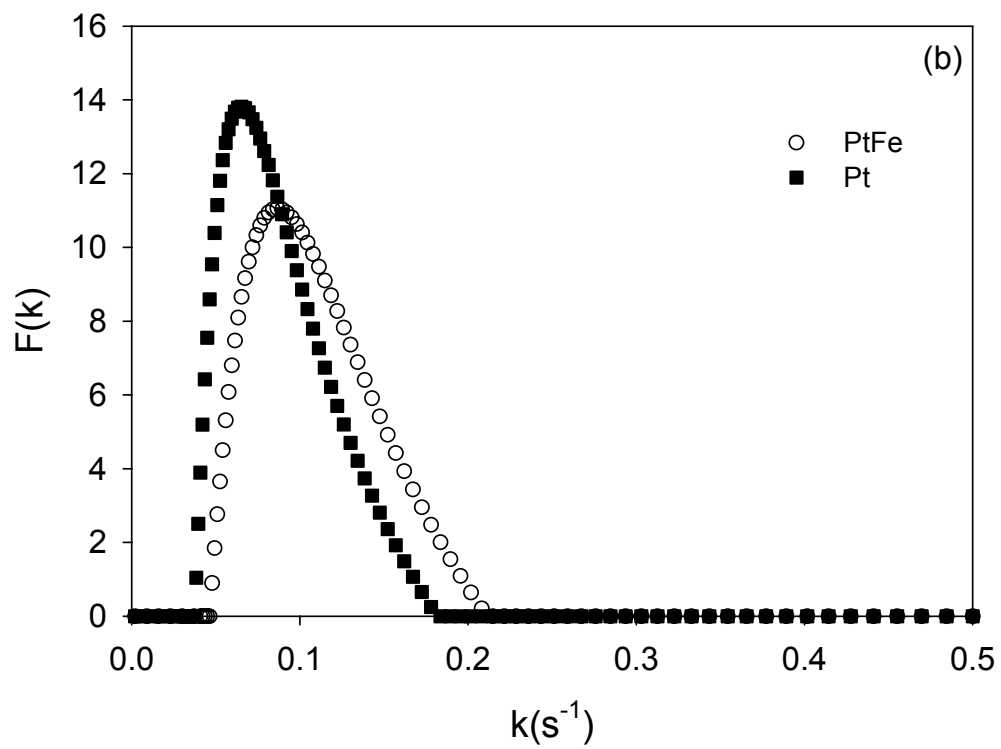
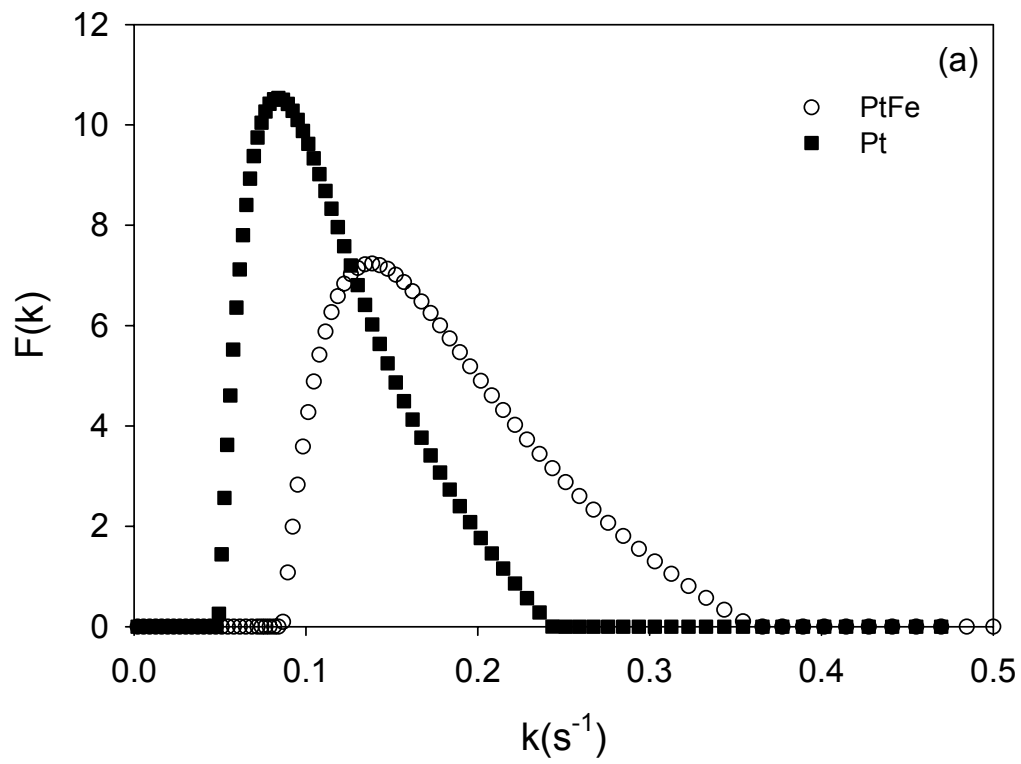


Figure C.9



APPENDIX D NCSU PULSE CHEMISORPTION FIGURES

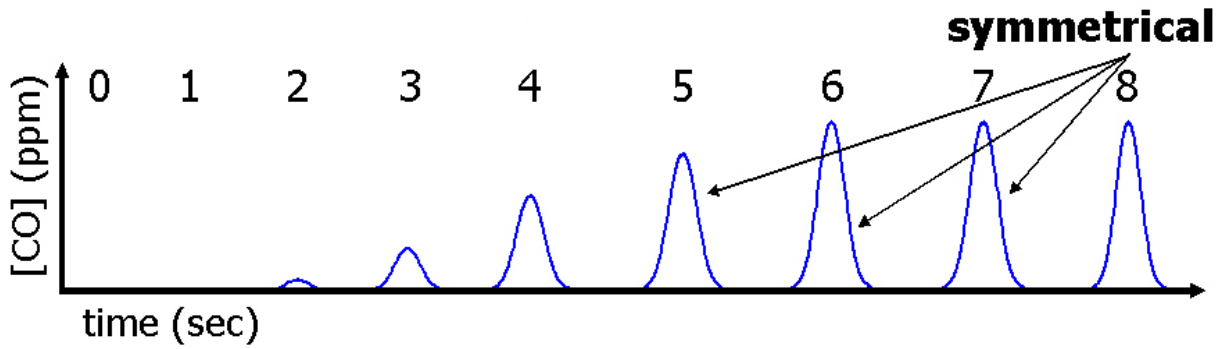


Figure D.1: Graphical representation of a theoretical pulse chemisorption test

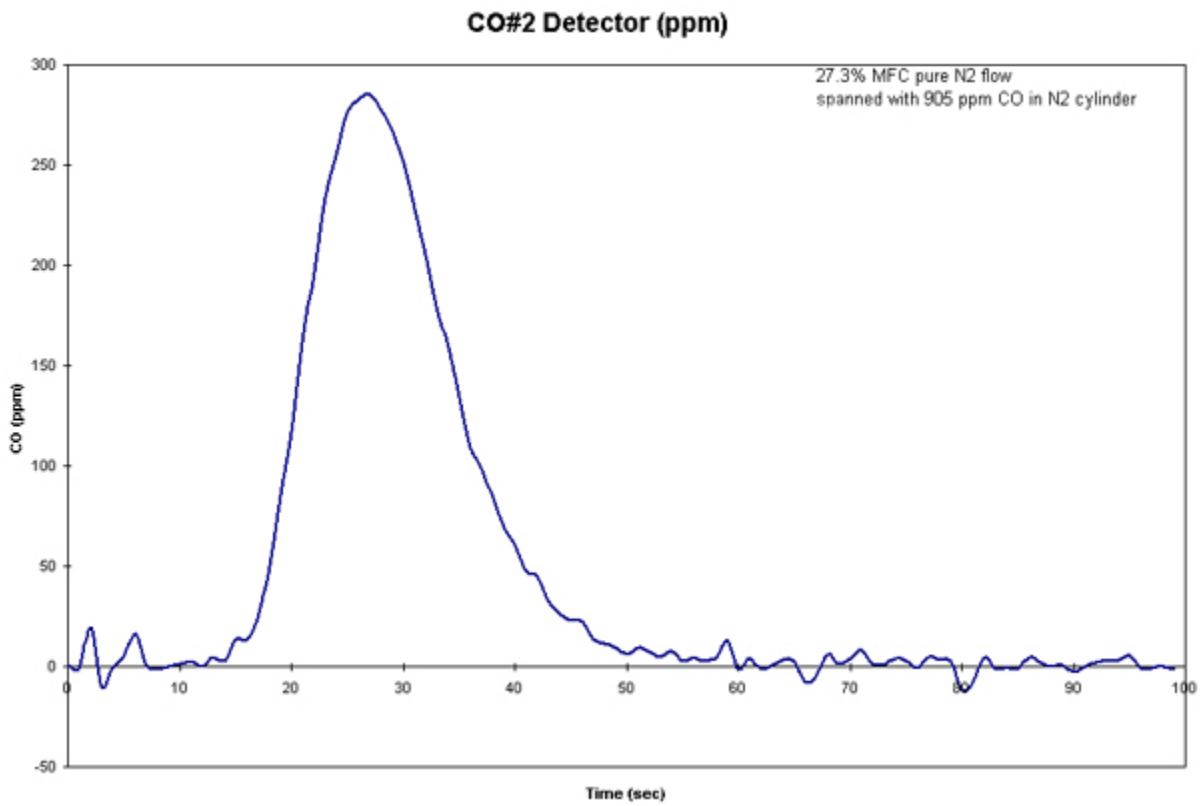


Figure D.2: Graphical representation of a typical theoretical pulse chemisorption data.

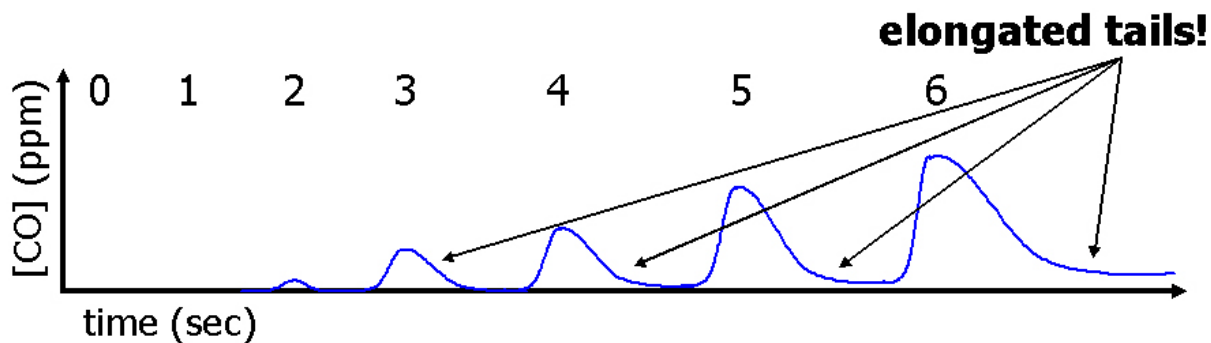


Figure D.3: Graphical representation of a pulse chemisorption test with elongated tails

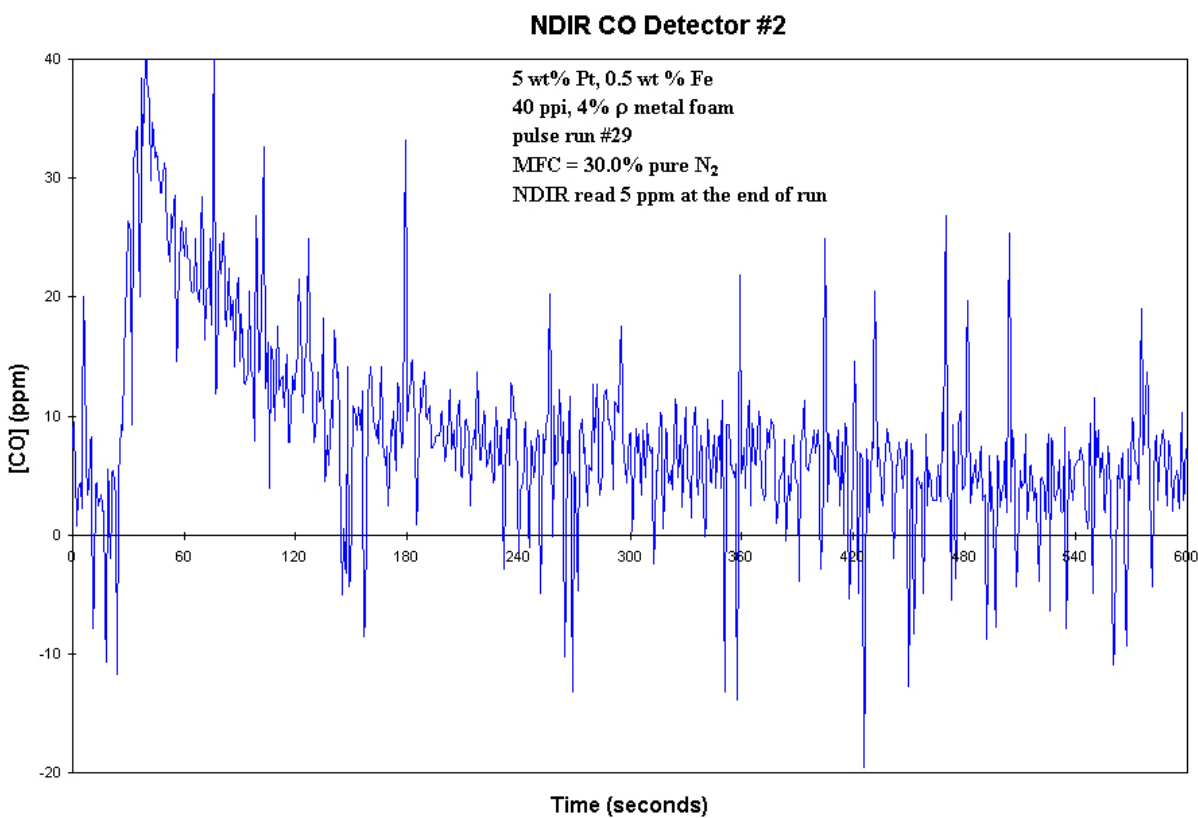


Figure D.4: Graphical representation of an elongated pulse chemisorption data.

Date	Type	Catalyst Loading	sample loop size	# pulses run	N ₂ Flow Rates	"Standard" Peak Error	Other Comments
08/28/03	Blank Reactor	No support	1 mL	10 pulses	(constant) 1.0 L/min	~1% error (1.0 L/min)	zeroed NDIR; last recorded span on NDIR was 15th August 2003
09/11/03	Blank Foam	No catalyst No washcoat	1 mL	16 pulses <i>8 each</i>	1.5 L/min 1.0 L/min	17% error (1.5 L/min) 5% error (1.0 L/min)	spanned NDIR night before w/ 203 ppm CO in N2
09/16/03	Blank Foam	No catalyst No washcoat	1 mL	16 pulses <i>8 each</i>	1.0 L/min 1.5 L/min	6% error (1.0 L/min) 15% error (1.5 L/min)	spanned NDIR night before w/ 203 ppm CO in N2
09/24/03	Blank Reactor	No support	1 mL	30 pulses <i>10 each</i>	1.0 L/min 1.5 L/min 2.0 L/min	6% error (1.0 L/min) 12.4% error (1.5 L/min) 19.5% error (2.0 L/min)	spanned NDIR w/ 203 ppm CO in N2 before each set of 10 pulses
10/14/03	Blank Foam	No catalyst No washcoat	1 mL	30 pulses <i>10 each</i>	1.5 L/min 1.0 L/min 1.5 L/min	21.5% error (1.5 L/min) 11.5% error (1.0 L/min) 21.3% error (1.5 L/min)	spanned NDIR w/ 203 ppm CO in N2 before pulsing Gas Chiller unplugged -- error larger without gas chiller plugged in
12/15/03	Blank Foam	No catalyst No washcoat	1 mL	43 pulses	1.0 L/min 1.5 L/min 1.0 L/min 1.5 L/min 1.0 L/min	<i>pulses 1-10</i> 9.3% error (1.0 L/min) <i>pulses 11-20</i> 18% error (1.5 L/min) <i>pulses 21-30</i> 18.7% error (1.0 L/min) <i>pulses 31-40</i> 30% error (1.5 L/min) <i>pulses 4-43</i> 8% error (1.0 L/min)	1-20 pulse used 905 ppm CO in N2 to span NDIR 21-40 pulse used 203 ppm CO in N2 to span NDIR 41-43 pulse used 905 ppm CO in N2 to span NDIR

Table D.1: Uncatalysed, unwashed blank foam and blank reactor data

* (Table D.1) No CO adsorption occurred in any of the blank reactor and blank foam runs

Date	Catalyst ID	sample loop size	N ₂ Flow Rates	Active Metal (chemisorption)	Metal Dispersion (chemisorption)	Other Comments
09/18/03	440-17-8D (40 ppi, 4% ρ) "newer" piece	1 mL	1.0 - 2.0 L/min	0.277-0.287% 0.304-0.305% (<i>edit</i>)*	5.04-5.22% 5.53-5.54% (<i>edit</i>)*	spanned NDIR w/ 203 ppm CO in N2 before pulsing 1.0 to 1.16 to 1.22 to 1.32 to 1.5 to 2.0 L/min pure N2
09/22/03	440-17-8D (40 ppi, 4% ρ) "newer" piece	1 mL	(<i>constant</i>) 1.5 L/min	0.360-0.367%	6.55-6.67%	spanned NDIR w/ 203 ppm CO in N2 before pulsing Reached 75-87% of 'standard' peak
09/25/03	E055-02P-404-7A (40 ppi, 4% ρ) "older" piece	1 mL	1.5 L/min 1.65 L/min	0.240-0.247% 0.371-0.373% (<i>edit</i>)*	4.37-4.50% 6.75-6.77% (<i>edit</i>)*	spanned NDIR w/ 203 ppm CO in N2 before pulsing recalibrated NDIR twice while running
10/01/03	E055-02P-404-7A (40 ppi, 4% ρ) "older" piece	5 mL (#1) 2 mL (#2)	(<i>constant</i>) 1.5 L/min	0.330-0.332% 0.453-0.454% (<i>edit</i>)*	6.00-6.04% 8.23-8.25% (<i>edit</i>)*	spanned NDIR w/ 203 ppm CO in N2 before pulsing recalibrated NDIR once while running

Table D.2: 'Identical' pieces of metal foam intracomparison

* Edited values take into account the negative difference when $n_{CO, loop}$ and $n_{CO, NDIR pulse}$ are subtracted from each other because of the positive error the NDIR gives when integrating the area under the ppm vs. time curve, giving greater value than $n_{CO, loop}$.

** (Table D.2) All catalyst are 5 wt% Pt, 0.5 wt% Fe; 40 ppi, 4% ρ metal foams

Date	Catalyst ID	sample loop size	N ₂ Flow Rates	Active Metal (chemisorption)	Metal Dispersion (chemisorption)	Other Comments
09/25/03	E055-02P-404-7A (40 ppi, 4% ρ) "older" piece	1 mL	1.5 L/min 1.65 L/min	0.240-0.247% 0.371-0.373% (<i>edit</i>)*	4.37-4.50% 6.75-6.77% (<i>edit</i>)*	spanned NDIR w/ 203 ppm CO in N2 before pulsing recalibrated NDIR twice while running
10/01/03	E055-02P-404-7A (40 ppi, 4% ρ) "older" piece	5 mL (#1) 2 mL (#2)	(<i>constant</i>) 1.5 L/min	0.330-0.332% 0.453-0.454% (<i>edit</i>)*	6.00-6.04% 8.23-8.25% (<i>edit</i>)*	spanned NDIR w/ 203 ppm CO in N2 before pulsing recalibrated NDIR once while running
10/17/03	E055-02P-2012-6A (20 ppi, 12% ρ)	2 mL (#1) 1 mL (#2)	(<i>constant</i>) 1.0 L/min	0.835-0.847% 0.848-0.853% (<i>edit</i>)*	15.18-15.40% 15.40-15.50% (<i>edit</i>)*	spanned NDIR w/ 203 ppm CO in N2 before pulsing First 9 pulses adsorbed using 2 mL sample loop Gas chiller not plugged in
10/21/03	E055-02P-2012-6A (20 ppi, 12% ρ)	2 mL (#1) 1 mL (#2)	(<i>constant</i>) 1.0 L/min	0.424-0.430% 0.462-0.463% (<i>edit</i>)*	7.71-7.82% 8.39-8.43% (<i>edit</i>)*	spanned NDIR w/ 203 ppm CO in N2 before pulsing Gas chiller not plugged in
10/24/03	E055-02P-2012-6A (20 ppi, 12% ρ)	2 mL (#1) 1 mL (#2)	(<i>constant</i>) 1.0 L/min	0.602-0.575% 0.454-0.457% (<i>edit</i>)*	10.94-10.46% 8.25-8.30% (<i>edit</i>)*	spanned NDIR w/ 203 ppm CO in N2 before pulsing chemisorption values cycled every couple of runs Never reached standard peak Gas chiller not plugged in
10/29/03	E055-02P-2012-6A (20 ppi, 12% ρ)	1 mL	(<i>constant</i>) 1.0 L/min	0.549-0.552% 0.583% (<i>edit</i>)*	9.99-10.04% 10.60% (<i>edit</i>)*	spanned NDIR w/ 203 ppm CO in N2 before pulsing chemisorption values cycled every couple of runs Gas Chiller plugged in

Table D.3: Comparison of 5 wt% Pt / 0.5 wt% Fe, varying ppi and ρ metal foams

* Edited values take into account the negative difference when $n_{CO, loop}$ and $n_{CO, NDIR pulse}$ are subtracted from each other because of the positive error the NDIR gives when integrating the area under the ppm vs. time curve, giving greater value than $n_{CO, loop}$.

Date	Catalyst ID	Catalytic Metal Loading	sample loop size	N ₂ Flow Rates	Active Metal (chemisorption)	Metal Dispersion (chemisorption)	Other Comments
09/10/03	E051-02P-40017C (400 cpsi)	5% Pt 0.05% Fe	1 mL	1.0 L/min 1.5 L/min	0.275%	5.44-5.45%	spanned NDIR night before w/ 203 ppm CO in N2 Reached 95% of peak after switched N2 flow rate from 1.0 to 1.5 L/min pure N2
10/09/03	E051-02P-40017A (400 cpsi)	5% Pt 0% Fe	2 mL (#1) 1 mL (#2)	(constant) 1.0 L/min	0.338-0.349% 0.395-0.399% (<i>edit</i>)*	6.75-6.98% 7.91-7.98% (<i>edit</i>)*	spanned NDIR w/ 203 ppm CO in N2 before pulsing Final 25-30% over peak at 1.0 L/min pure N2 Gas Chiller unplugged

Table D.4: Comparison of 5 wt% Pt, varying Fe loading ceramic monoliths

* Edited values take into account the negative difference when $n_{CO, loop}$ and $n_{CO, NDIR pulse}$ are subtracted from each other because of the positive error the NDIR gives when integrating the area under the ppm vs. time curve, giving greater value than $n_{CO, loop}$.

** (Table D.4) All catalysts are 400 cpsi, 5 wt% Pt ceramic straight-channel monoliths

APPENDIX E NCSU TPD FIGURES

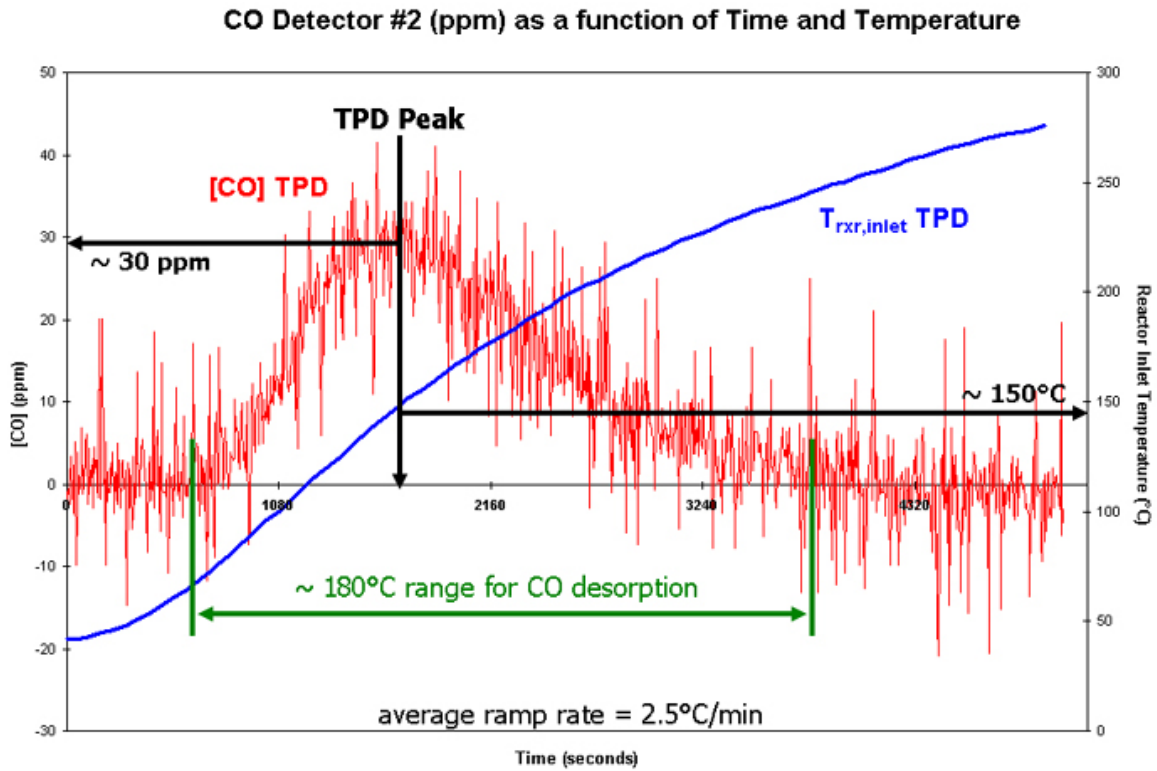


Figure E.1: Typical graphical representation of TPD data.

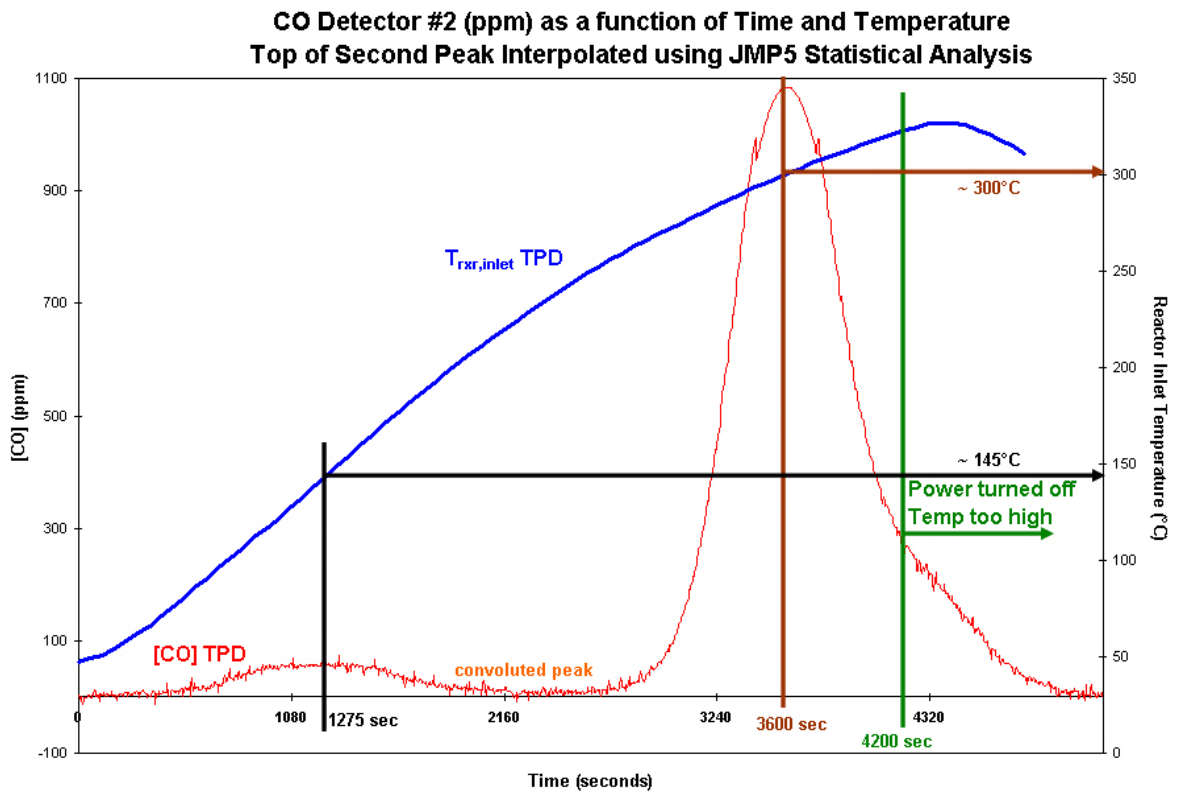


Figure E.2: Bimodal peak TPD graph for the 20 ppi, 12% ρ metal foam, trial one

Date	Catalyst ID	N ₂ Flow Rates	Ramp Rate (°C/min) average	Ramp Rate (°C/min) linear fit	Active Pt (TPD)	Dispersion for Pt	Avg Pt Diameter Size	T _{des}	Other Comments
09/18/03	440-17-8D (40 ppi, 4% ρ) "newer" piece	--	--	--	--	--	--	--	
09/22/03	440-17-8D (40 ppi, 4% ρ) "newer" piece	--	--	--	--	--	--	--	
09/25/03	E055-02P-404-7A (40 ppi, 4% ρ) "older" piece	--	--	--	--	--	--	--	
10/01/03	E055-02P-404-7A (40 ppi, 4% ρ) "older" piece	(constant) 1.0 L/min	2.82 (in)* 2.31 (out)	3.05 (in)* 2.46 (out)	0.232% to 0.235%	4.65% to 4.69%	260 Å to 258 Å	150°C	spanned NDIR w/ 203 ppm CO in N2 before TPD

Table E.1: 'Identical' pieces of metal foam intracomparison

** (Table E.1) All catalyst are 5 wt% Pt, 0.5 wt% Fe; 40 ppi, 4% ρ metal foams

Date	Catalyst ID	Catalytic Metal Loading	N ₂ Flow Rates	Ramp Rate (°C/min) average	Ramp Rate (°C/min) linear fit	Active Pt (TPD)	Dispersion for Pt (TPD)	Avg Pt Diameter Size (TPD)	T _{des}	Other Comments
09/10/03	E051-02P-40017C (400 cps)	5% Pt 0.05% Fe	--	--	--	--	--	--	--	spanned NDIR w/ 203 ppm CO in N2 before TPD
10/10/03	E051-02P-40017A (400 cps)	5% Pt 0% Fe	(constant) 1.0 L/min	2.60 (in)* 2.16 (out)	2.79 (in)* 2.30 (out)	0.231-0.227%	4.62-4.54%	262-267 Å	136°C	spanned NDIR w/ 203 ppm CO in N2 before TPD Gas chiller unplugged

Table E.2: Comparison of 5 wt% Pt, varying Fe loading ceramic monoliths

*** (Table E.2) All catalysts are 400 cps, 5 wt% Pt ceramic straight-channel monoliths

* "in" values represent ramp rates calculated at the reactor inlet temperature; "out" values represent ramp rates calculated at the reactor outlet temperature

Date	Catalyst ID	N ₂ Flow Rates	Ramp Rate (°C/min) average	Ramp Rate (°C/min) linear fit	Active Pt (TPD)	Dispersion for Pt (TPD)	Avg Pt Diameter Size (TPD)	T _{des}	Other Comments
09/25/03	E055-02P-404-7A (40 ppi, 4% ρ) "older" piece	--	--	--	--	--	--	--	
10/07/03	E055-02P-404-7A (40 ppi, 4% ρ) "older" piece	(constant) 1.0 L/min	2.82 (in)* 2.31 (out)	3.05 (in)* 2.46 (out)	0.232% to 0.235%	4.65% to 4.69%	260 Å to 258 Å	145°C	spanned NDIR w/ 203 ppm CO in N2 before TPD spanned NDIR w/ 203 ppm CO in N2 before TPD
10/18/03	E055-02P-2012-6A (20 ppi, 12% ρ)	(constant) 1.0 L/min	3.94 (in)* 4.28 (out)	3.80 (in)* 4.22 (out)	Peak #1: 0.336% Peak #2: 4.697% Total (spline): 5.03%	Peak #1: 6.714% Peak #2: 93.944% Total (spline): 100.66%	Peak #1: 180.23 Å Peak #2: 12.88 Å Total (spline): 12.02 Å	145°C 300°C	TPD had Bimodal peak Peak #1 ~ 145°C Peak #2 ~ 300°C Gas chiller unplugged
10/22/03	E055-02P-2012-6A (20 ppi, 12% ρ)	(constant) 1.0 L/min	4.98 (in)* 4.88 (out)	5.37 (in)* 5.57 (out)	0.243-0.245%	4.87-4.90%	247-249 Å	155°C	spanned NDIR w/ 203 ppm CO in N2 before TPD Tried to reproduce prior run Only one peak in TPD Gas chiller unplugged
10/25/03	E055-02P-2012-6A (20 ppi, 12% ρ)	(constant) 1.0 L/min	4.60 (in)* 4.55 (out)	4.90 (in)* 5.15 (out)	0.536-0.538%	10.73-10.69%	113 Å	178°C	spanned NDIR w/ 203 ppm CO in N2 before TPD TPD never went to zero (read 5 ppm @ end) Gas chiller unplugged
10/30/03	E055-02P-2012-6A (20 ppi, 12% ρ)	(constant) 1.0 L/min	5.47 (in)* 5.40 (out)	5.82 (in)* 6.11 (out)	0.275-0.285%	5.50-5.69%	220-213 Å	155°C	spanned NDIR w/ 203 ppm CO in N2 before TPD TPD flooded @ 2 L/min 10% CO/N2 to see if faster flow rate effects mass transfer & adsorption Gas chiller plugged in
12/19/03	E054-02P-4012A (40 ppi, 12% ρ)	(constant) 1.0 L/min	3.14 (in)* 3.47 (out)	2.96 (in)* 3.12 (out)	0.453-0.460%	8.24-8.36%	147-145 Å	113- 128°C	spanned NDIR w/ 905 ppm CO in N2 before TPD

Table E.3: Comparison of 5 wt% Pt / 0.5 wt% Fe, varying ppi and ρ metal foams

* "in" values represent ramp rates calculated at the reactor inlet temperature; "out" values represent ramp rates calculated at the reactor outlet temperature